

CHALMERS



Start capability of industrial synchronous motor with high efficiency

Master's Thesis in Electrical Power Engineering

DANIEL PEHRMAN & MATHIAS JONES

Department of Energy & Environment
Electric Power Engineering
CHALMERS UNIVERSITY OF TECHNOLOGY
Gothenburg, Sweden 2014
Master's Thesis 2014:1

Abstract

This thesis includes an investigation of the starting capability of a high efficiency synchronous motor for direct on-line industrial applications. The approach is to use a hybrid rotor concept to achieve the starting properties of an induction motor and the steady state performance of a synchronous reluctance motor. The hybrid motor rated at 20 kW is compared and evaluated against a same size induction motor in aspect to parameter variations. Simulations showed that the rotor losses can be reduced by 80 % in the best case. The total motor losses decrease by 20-30 %. This gain in efficiency will improve the efficiency class of the motor from IE3 to IE4. Furthermore, the results from this thesis hopes to raise the interest in investigation of new line-start, high efficiency motors further.

Keywords: line-start, direct on-line, high efficiency, synchronous reluctance motor (SynRM), induction motor (IM), rotor design, FEM, benchmarking.

Acknowledgements

The authors would like to thank Prof. Yujing Liu for his expertise and guidance in this project, Dr. Freddy Gyllensten and Dr. Iakovos Manola for helpful suggestions and insight. Also a grateful thanks to Dr. Pär Ingelström and Dr. Johan Åström for their knowledge and help with the simulations.

The Authors, Gothenburg 10/6/2014

Contents

Nomenclature	iii
1 Introduction	1
1.1 Background	1
1.2 Efficiency classes	2
1.3 Aim	3
1.4 Previous studies within the field	3
1.5 Thesis structure	3
2 Induction Motor	4
2.1 History and Development	4
2.2 Basic Working Principle	4
2.3 Stator design	7
2.4 Rotor design	7
2.5 Loss distribution	8
3 Synchronous reluctance motor	10
3.1 History of the synchronous reluctance motor	10
3.2 Basics	10
3.3 Rotor design	12
3.3.1 Placement of air barriers and iron paths	12
3.3.2 Saliency ratio	14
3.4 Start-up	16
3.5 Efficiency	17
4 Hybrid rotor modelling	18
4.1 Hybrid concept	18
4.2 Simulation setup	19
4.2.1 Rotor parameters	20
4.3 Verification	23

4.3.1	Meshing	23
4.3.2	Time step	25
5	Simulation results	28
5.1	Start-up	28
5.2	Steady state	37
5.3	Promising designs	45
5.3.1	Hybrid-1, circular cage	45
5.3.2	Hybrid-2, elliptic cage	45
5.4	Performance summary	50
6	Conclusion	51
6.1	Discussion	52
6.2	Future Work	52
A	Induction Machine data for analytical solution	53
	Bibliography	59

Nomenclature

FEM	Finite element method
IEC	International electrotechnical commission
IM	Induction machine
IPF	Internal Power factor
LS-SynRM	Line-start synchronous reluctance motor
ME	Maximum efficiency
MMF	Magnetomotive force
MPF	Maximum power factor
MTPA	Maximum torque per ampere
MTPkVA	Maximum torque per kVA
PF	Power factor
PM	Permanent magnet
SCIM	Squirrel cage induction motor
SynRM	Synchronous reluctance motor
VSD	Variable speed drive

1

Introduction

1.1 Background

The key aspects in sustainable energy development is to harvest renewable energy but also to use the energy more efficiently. About 40 % of electricity produced is used by electrical motors with the average efficiency of 88 %. The remaining energy loss corresponds globally to 0.5 billion tons of CO₂ emission every year. A challenge within the field of motor development is to make motors more efficient while maintaining a low cost and robustness.

The induction machine (IM) has long been the most utilized electrical motor in the industry because of its robustness and low price. Since it runs at asynchronous speed the efficiency is limited by its slip created between the rotor and stator fields. The currents that are induced in the rotor windings cause unnecessary losses. These losses are called rotor copper losses.

ABB have developed a synchronous reluctance motor (SynRM) that can compete with the robustness and low price of the IM and at the same time has higher efficiency. In the SynRM the copper losses in the rotor are eliminated which corresponds to a reduction of the losses by up to 40 % [1].

However, the SynRM has no or little torque when deviating from the synchronous speed so a frequency converter or a starting motor is needed in order start a synchronous motor. A hybrid arrangement between the IM and the SynRM could combine the direct-online starting from the IM with the high steady state efficiency of the SynRM. This hybrid motor is supposed to have the capability to start without any external starting device

and have high efficiency during steady state operation.

Constant speed applications are common in the industry. For these types of applications the hybrid motor can replace many of the existing IM's, especially in the low and middle power ranges. If the motor losses were reduced by 40 % the CO₂ emissions would be reduced by 200 million tons of CO₂ emissions every year. This corresponds to Sweden's total CO₂ emissions for a 3 years period [2].

1.2 Efficiency classes

In 2009 the EU commission implemented a new directive called EN 60034-30:2009 which divides electrical rotating motors in classes depending on power output and efficiency. The different classes ranges from IE1 which is standard efficiency to IE4 which is super premium efficiency. Even a new class called IE5, ultra premium efficiency is under development. For each efficiency class the losses are reduced by 20 %. In Figure 1.1 the different classes are illustrated for a 4-pole, 50 Hz motor. The directive from 2009 states among other things that from 2015 the lowest efficiency class manufactured in the European Union shall be IE3 [3].

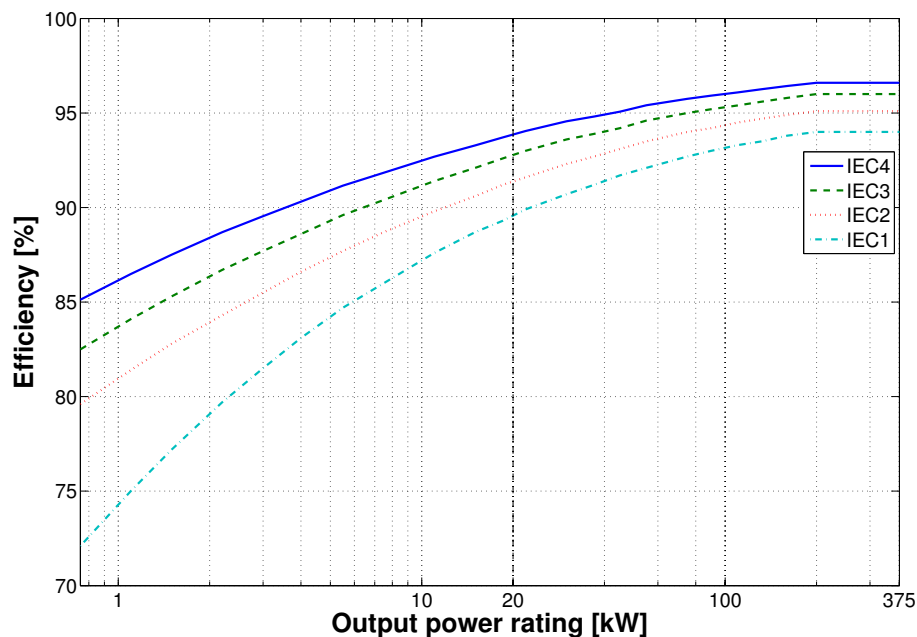


Figure 1.1: IEC 60034-30 efficiency standard for a 4-pole, 50 Hz motor.

1.3 Aim

The aim of this thesis work is to investigate the possibilities with a hybrid arrangement between the IM and the SynRM by adding a squirrel cage to the rotor of a SynRM. The hybrid arrangement will be evaluated regarding direct-on-line starting and steady state performance.

1.4 Previous studies within the field

Self starting synchronous machines have become a hot topic in the area of motor design. There are several articles and studies that have been made in the field. In the area of cage assisted synchronous machines there are some facts that can be concluded.

The starting performance is depending on position of the bar placement [4].

Experimental validation of the start has been made and concluded that it can compete with the IM both in efficiency and power factor. The FEM simulations were consistent with the experimental result and seems to work as an accurate design environment [5].

There have been some problems with pulsating torque during steady state making the motor unstable [6].

1.5 Thesis structure

The thesis is divided into five parts. Chapter 1 is an introduction to the field and motivation of the thesis and also a vision of the potential benefits gained with a successful design. It also contains the aim of the thesis and previous work done in related topics. The purpose of Chapter 2 and 3 is to introduce some basic concepts for the reader to better understand the following chapters and present the two motor types. Chapter 2 and 3 aims also to introduce benefits and disadvantages with the two motor types.

Chapter 4 describes theoretically the concepts for the hybrid arrangement. Furthermore, the simulation modelling and validation is covered in this chapter.

Chapter 5 presents the simulation results about the different design variations introduced in Chapter 4. This chapter is the backbone of the thesis. Lastly, in Chapter 6 the conclusions are presented together with future improvements and a discussion.

2

Induction Motor

2.1 History and Development

In 1831 Faraday published the electromagnetic law of induction and around 1860 Maxwell formulated the equations for electricity, Maxwell's equations. This knowledge was essential for the invention of the induction motor. In 1885 Galileo Ferrari's and one year afterwards (1886) Nikola Tesla presented two types of motors where the operating principle can be recognized in to days IM's. A rotating magnetic field in the stator induces currents in rotor bars or windings that produces the torque of the motor.

This principle was taken to industrial use by Dolivo-Dobrovolsky whom also invented the wound and cage rotor around year 1889 and in 1900 the motor was ready for wide industrial use. One of the key benefits of the IM is the non-zero torque at zero speed which means that it is self-starting. This allow the motor to be grid connected without an external starting device. The IM has been known to be called "the work horse" of the industry since its introduction in the industry and with modern technology the IM have improved in all areas and has reached its peak in performance regarding efficiency and power density [7].

2.2 Basic Working Principle

A typical IM consists of a multiphase stator winding that produce a traveling magnetic field that induces current in short circuited windings or bars in the rotor, see Figure 2.3.

The induced current produces the torque of the motor. In order for the motor to generate active torque there needs to be a speed difference between the rotating electric field in the stator and the speed of the rotor known as slip, s . This slip is defined in equation (2.1) and is causing ohmic losses in the rotor during steady state that is proportional to the slip times the output power of the motor. In Figure 2.1 the equivalent schedule of the IM can be seen.

$$s \equiv \frac{\omega - \omega_r}{\omega} \quad (2.1)$$

Where ω is the synchronous speed and ω_r is the rotor speed.

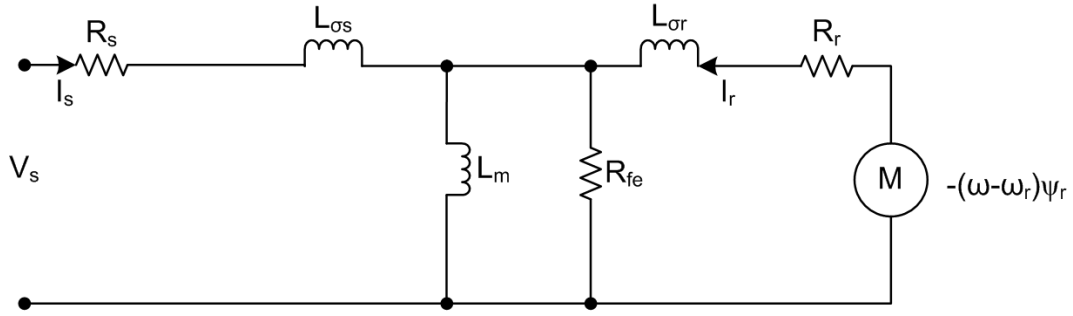


Figure 2.1: Equivalent circuit for the IM.

Where \underline{V}_s is the stator voltage and \underline{I}_s the stator current (underscore means phasor representation), R_s is the stator winding resistance and $L_{\sigma s}$ represents the stator winding inductance. L_m is the mutual inductance and R_{fe} is the ohmic iron losses. $L_{\sigma r}$ is the rotor bar inductance and R_r represents the rotor bar resistance. $\underline{\psi}_s$ and $\underline{\psi}_r$ is the stator and rotor flux. T_e is the moving torque acting to rotate the motor.

The steady state equations for the induction motor can be derived from Figure 2.1 and are presented in (2.2)-(2.5).

$$\underline{V}_s = R_s \underline{I}_s + j\omega(L_m(\underline{I}_s + \underline{I}_r)) + j\omega L_{\sigma s} \underline{I}_s \quad (2.2)$$

$$0 = \frac{R_r}{s} \underline{I}_r + j\omega L_m(\underline{I}_s + \underline{I}_r) + j\omega L_{\sigma r} \underline{I}_r \quad (2.3)$$

$$\underline{\psi}_s = L_m(\underline{I}_s + \underline{I}_r) + L_{\sigma s} \underline{I}_s \quad (2.4)$$

$$\underline{\psi}_r = L_m(\underline{I}_s + \underline{I}_r) + L_{\sigma r}\underline{I}_r \quad (2.5)$$

$$T_e = \frac{3n_p}{2} \text{Im} \{ \underline{\psi}_s^* \underline{I}_s \} = \frac{3n_p}{2} \text{Im} \{ L_m \underline{I}_r^* \underline{I}_s \} = \frac{3n_p}{2} \text{Im} \{ \underline{\psi}_r \underline{I}_r^* \} \quad (2.6)$$

From these equations a characteristic torque curve for different speeds can be extracted, see Figure 2.2.

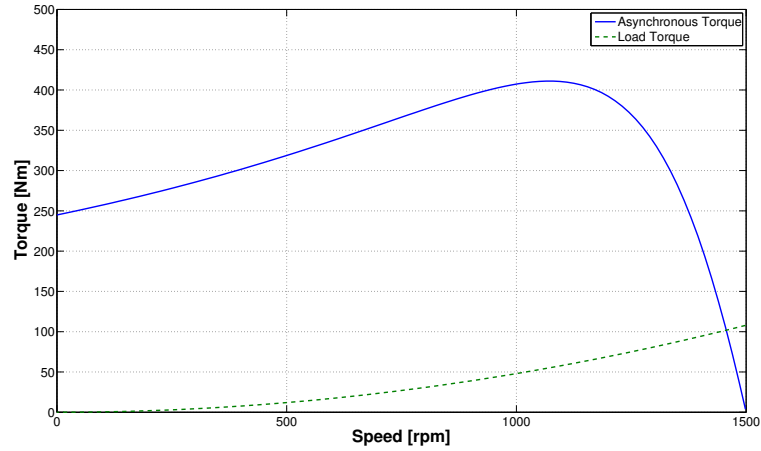


Figure 2.2: Torque speed curve for a typical IM with quadratic load torque.

In Figure 2.2 a typical IM torque characteristic can be seen together with a quadratic load characteristic. The motor will operate at the point of intersection which corresponds to a certain torque and speed.

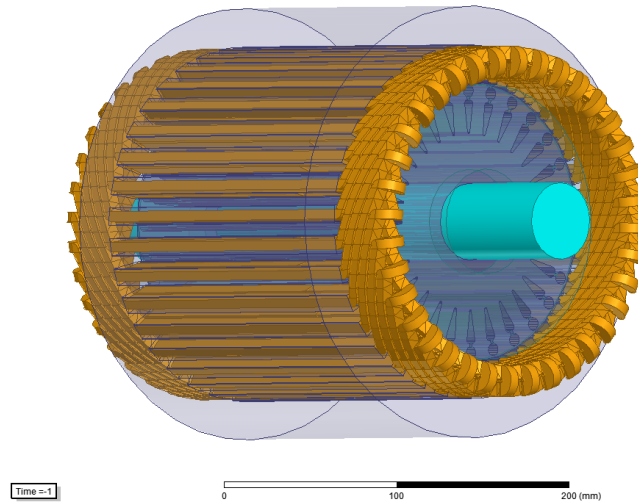


Figure 2.3: Squirrel cage induction motor.

The robustness, low cost and the ability of direct on-line starting have made the IM a common choice for constant speed applications but at lower power ratings especially between 5 kW - 30 kW the efficiency can be improved [8].

2.3 Stator design

The stator is made of laminated iron with slots of different shapes filled with copper or aluminum windings. Commonly, it has 2-6 poles and is operated from a three phase AC source.

In this thesis the focus will not be on the stator design. Any comparison between motors in this thesis will be made with the same stator. The stator used in the simulations in Chapter 5 is constructed as similar as possible with an existing motor, see Appendix A for detailed design specifications.

2.4 Rotor design

The rotor can either be constituted by windings or bars, leaving two categories, wound rotor and squirrel cage rotor. The squirrel cage rotor is the most common because of its simple design and variety. The squirrel cage is enclosed in laminated iron which makes the rotor very robust. [7]. In Figure 2.4 a typical squirrel cage can be seen. It consist of bars that are short circuited at the ends by so called end rings. The bar shape

and placement has a strong influence on the motor performance. It normally consist of aluminum but copper is also known to be used in high efficiency applications.

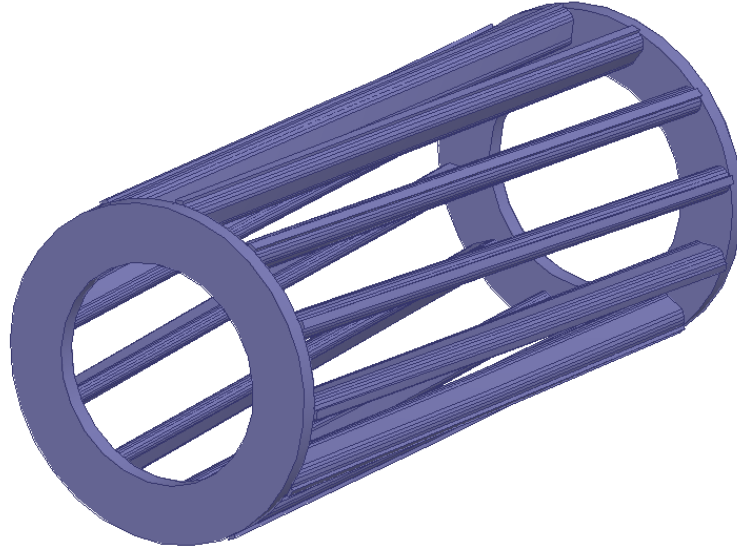


Figure 2.4: Typical squirrel cage with skew and end rings at both ends.

2.5 Loss distribution

With new tougher environmental guidelines the industry is pushed to more and more efficient motors. The highest class, IE4, is difficult for a middle size IM to reach.

In order to find a hybrid motor that can compete with the IM it is important to identify and localize the losses in the induction motor. They can be divided as follows:

- Stator copper losses, P_{Cu1}
- Rotor copper losses, P_{Cu2}
- Core iron losses, P_{fe1}
- Friction and windage losses, P_{mech}
- Stray losses, P_{stray}

The stator copper losses are the biggest source of losses in the motor. Next is the rotor copper losses and the core losses. The stray losses are due to eddy currents in the motor and are hard to localize. They vary from one design to another and are located both in the stator and rotor [8]. For an typical IM around 20 kW of output power the losses are distributed as depicted in figure 2.5 [1]. Other losses consist of core iron losses, friction losses, windage losses and stray losses.

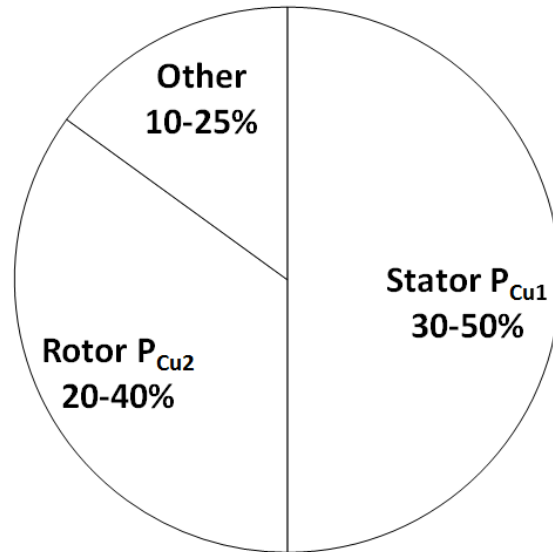


Figure 2.5: Typical loss distribution for an induction motor.

Since the stator for a IM and a SynRM are very similar it is in the rotor the biggest reduction of the losses can be made. Thus the thesis focus will be on reducing the rotor copper losses.

3

Synchronous reluctance motor

3.1 History of the synchronous reluctance motor

A traditional SynRM consist of a salient rotor with no coils. In 1923 J. K. Kostko showed the influence of the rotor design in his article "Polyphase Reaction Synchronous Motors" and presented concepts that highlighted the performance and potential of the SynRM [9]. The main benefits of the SynRM is the high efficiency, high torque density and no rare earth PM which gives a simple manufacturing. This chapter aims to give an insight in the design of a SynRM rotor.

3.2 Basics

Basically, the SynRM contains of an IM stator with a salient rotor. A salient rotor placed in a magnetic field will try to align with the field. The greater the difference in reluctance between an aligned rotor and a non-aligned rotor, the greater the produced torque will be. This phenomena is illustrated in Figure 3.1.

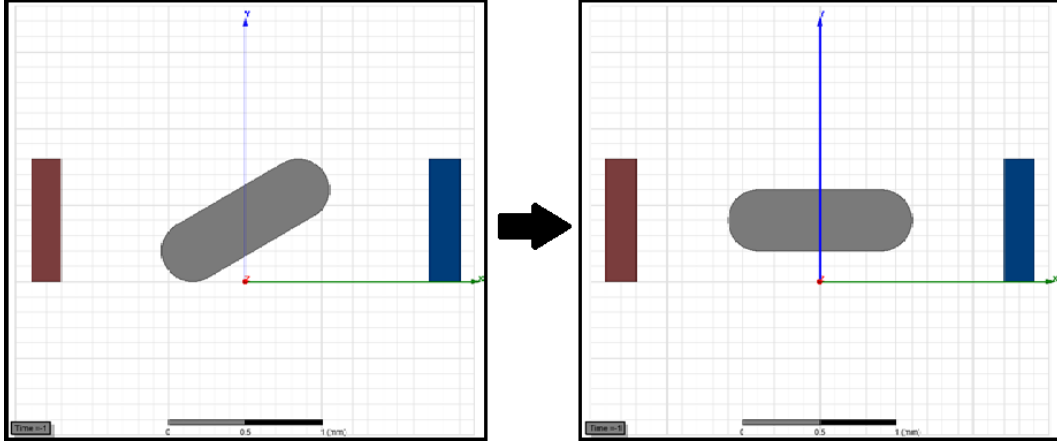


Figure 3.1: The concept of reluctance torque.

An equivalent circuit of the SynRM is shown in Figure 3.2.

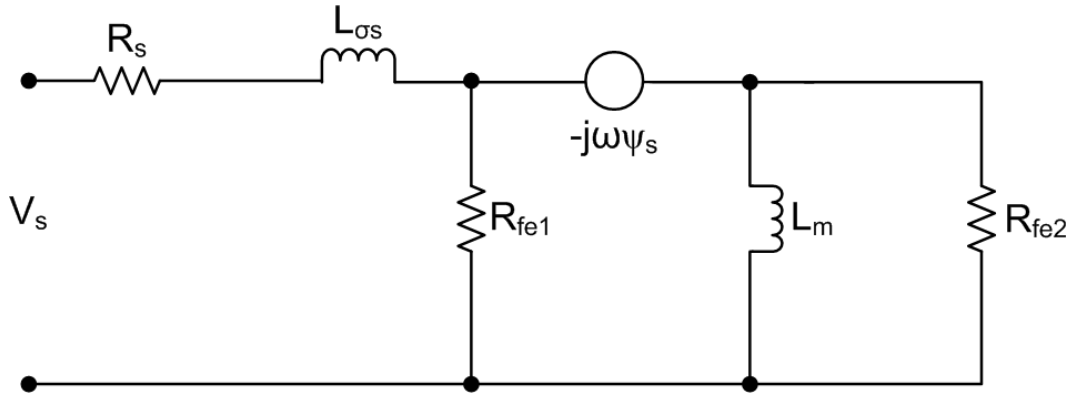


Figure 3.2: Equivalent circuit of the SynRM.

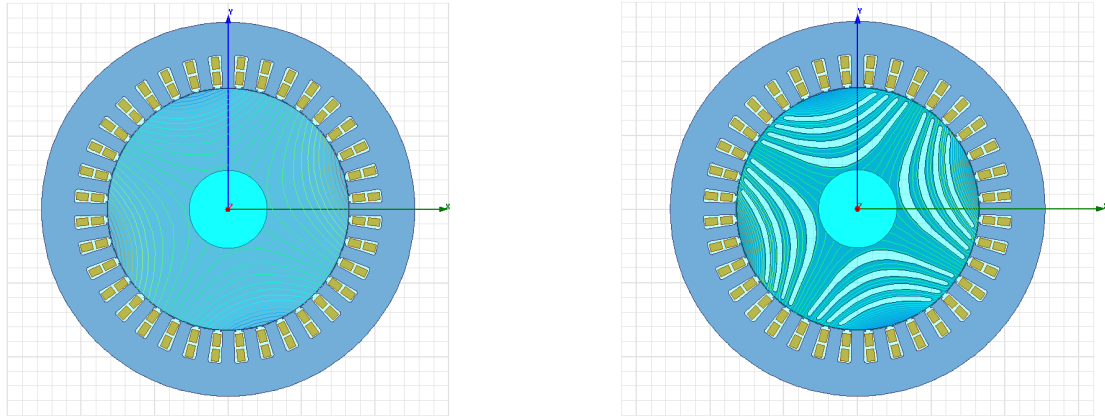
As seen from Figure 3.2, the equations that describes the relation between input voltage (V_s) and winding current (I_s) can be described by (3.1) [5].

$$\begin{aligned}
 v_{ds} &= r_s i_{ds} + \frac{d}{dt} L_{\sigma s} i_{ds} - \omega_r L_{qs} i_{qs} \\
 v_{qs} &= r_s i_{qs} + \frac{d}{dt} L_{\sigma s} i_{qs} - \omega_r L_{ds} i_{ds} \\
 \lambda_s &= L_s \cdot i_s \\
 V_s &= v_{ds} + j \cdot v_{qs} \\
 I_s &= i_{ds} + j \cdot i_{qs}
 \end{aligned} \tag{3.1}$$

Where r_s is the stator winding resistance, $L_{\sigma s}$ is the stator winding inductance, λ_s is the air gap linkage flux, L_m is the magnetic inductance and $R_{fe1,2}$ is the iron resistance in the stator and rotor respectively.

3.3 Rotor design

To achieve an effective rotor design a first step is to study the field lines in an isotropic core. The field lines can be approximated by hyperbolic curves. By introducing air barriers bounded by hyperbolic curves the flux in the d-axis will be unaffected while the q-axis flux will be blocked, see Figure 3.3a/3.3b. This method is an initial step towards a modern design of the SynRM rotor.



(a) Field lines with one phase excited in the stator for an isotropic rotor.

(b) Field lines with one phase excited in the stator for an aligned, non-isotropic rotor.

Figure 3.3: Design of the air barriers in the rotor.

3.3.1 Placement of air barriers and iron paths

The air barriers can be varied in number (k), thickness (B_0) and position (R_b). The purpose of the barriers is to block the q-axis flux in such a way that the d-axis flux is unaffected as much as possible. A first approach is to determine an optimal width for each path which will depend on the magneto motive force (MMF) in per unit (p.u.) where it is located. The higher the MMF the wider should both the barrier and path be. This is illustrated in Figure 3.4a/3.4b and more deeply evaluated in [10]. In order to avoid saturation in the iron it has to be wide enough depending on the absolute value of the field strength. Although, it is desirable to fit as much air as possible to keep the inductance in q-axis as low as possible while avoiding saturating the iron in the paths. In the above example the rotor slot pitch is constant between all barriers. By studying

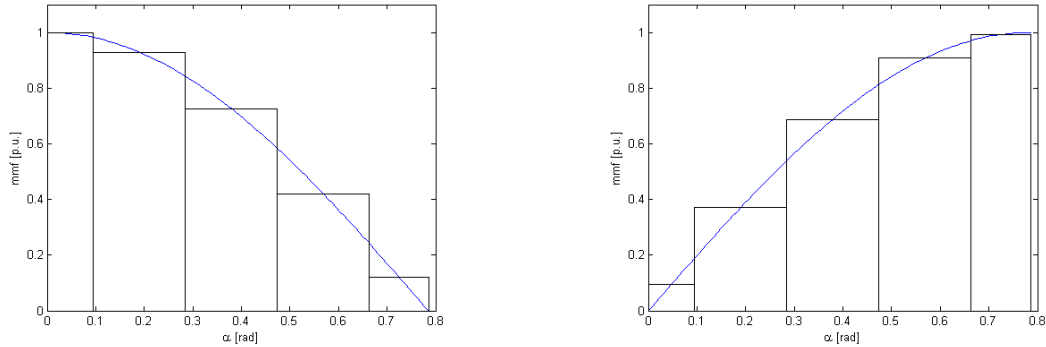
variation of the air/iron ratio, k_{wq} the width of barriers and paths will be varied and thus the performance of the motor. The relation of k_{wq} is presented in (3.2) where l_a is the amount of air and l_q is the amount of iron in the q-axis.

$$k_{wq} = \frac{l_a}{l_y} = \frac{\sum_{k=1}^n W_k}{\sum_{k=1}^n S_k + S_{n+1}} \quad (3.2)$$

where n is number of air barriers and W_k is the length of the k :th air barrier, S_k is the length of the k :th iron path and for a non-cut off structure; S_n is the length of the last iron path. This can be rewritten to (3.3).

$$k_{wq} = \frac{\left(\frac{D}{2} - \frac{D_{shaft}}{2} - d_{gap}\right) - \sum_{k=1}^{n+1} S_k}{\sum_{k=1}^{n+1} S_k} \quad (3.3)$$

where D is rotor diameter, D_{shaft} is shaft diameter and d_{gap} is air gap length between rotor and stator.



(a) MMF over paths when excited and positioned in d-axis.

(b) MMF over paths when excited and positioned in q-axis.

Figure 3.4: Width of the paths.

Next step is to determine where the center of each barrier should be located. By using (3.4) which comes from that the rotor slot pitch is constant, the center position for each barrier can be determined [10].

$$\alpha_m = \frac{\frac{\pi}{2p} - \beta}{k + 0.5} \quad (3.4)$$

Where β is the angle of the last path when using a cut-off rotor structure but for simplicity it is not considered in this thesis. A parametric plot of the center of each rotor barrier in a 4 barrier setup is shown in Figure 3.5.

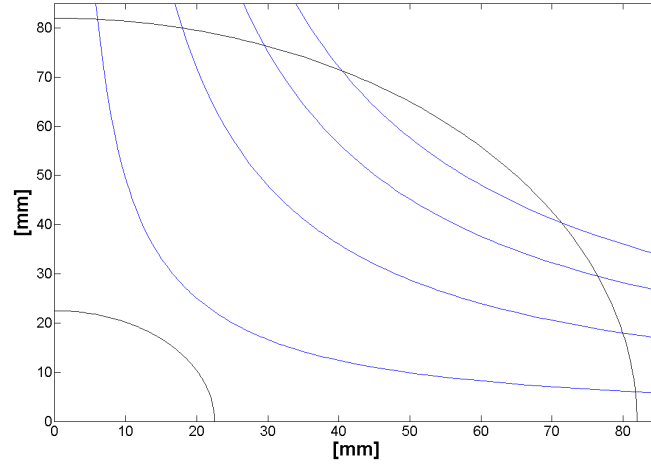


Figure 3.5: Center line for each air barrier in position to rotor diameter.

3.3.2 Salience ratio

The SynRM is developing torque through reluctance difference in the d- and q-axis. The ratio of the inductance in aligned and non-aligned position is an important performance parameter. This ratio (salience ratio) is defined as

$$\xi = \frac{L_d}{L_q}$$

The salience ratio is proportional to the maximum internal power factor according to (3.5) while the difference in inductance, $L_d - L_q$, is influencing the torque, see (3.6) [10]. The maximum internal power factor can be plotted for different salience ratio as seen in Figure 3.6.

$$IPF_{max} = \cos(\phi) = \frac{\xi - 1}{\xi + 1} \quad (3.5)$$

$$T_e = \frac{3P}{2} (L_d - L_q) i_{ds} i_{qs} \quad (3.6)$$

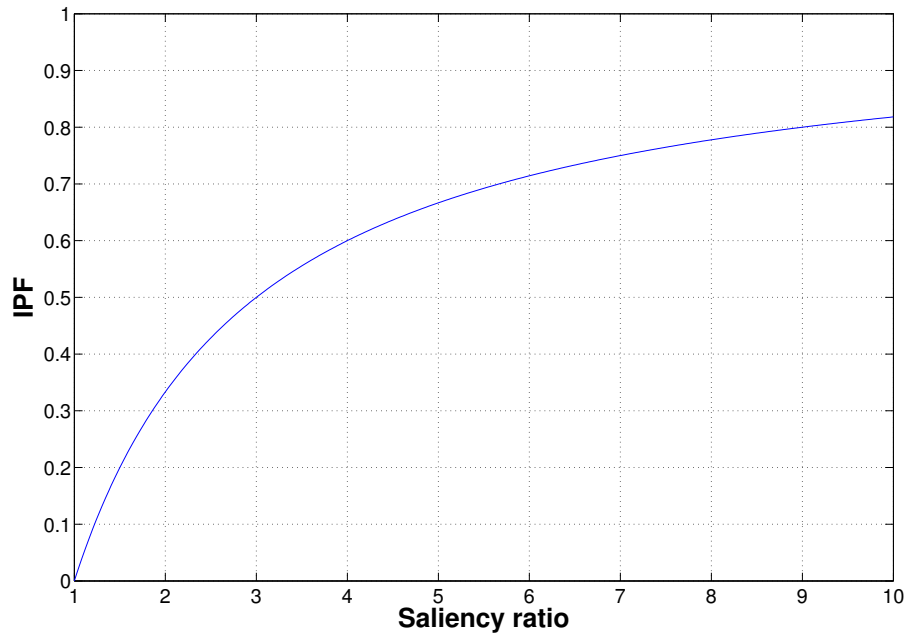


Figure 3.6: Maximum internal power factor as a function of saliency ratio.

Method to calculate the inductance

The inductance is calculated by applying a current to the stator winding and aligning the rotor. When the rotor is aligned the inductance is obtained from the stored energy by (3.7). Then by rotating towards the q-axis and calculating the energy stored in the rotor, the inductance over time can be plotted, see Figure 3.7.

$$W = \frac{1}{2}LI^2 \quad (3.7)$$

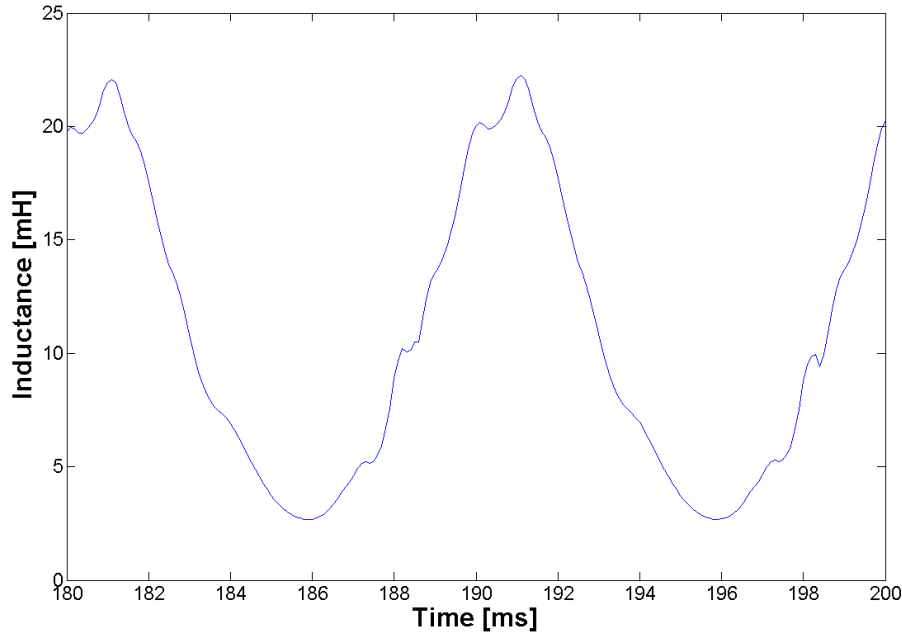


Figure 3.7: Inductance plotted when the rotor rotates enables the calculation of saliency ratio and saliency difference.

The minimum value of the inductance will be L_q and the maximum will be L_d . For the initial rotor design the saliency ratio was $\xi = 8.2$

Another method to determine the saliency ratio is by using (3.8) in a similar manner.

$$L_{d,q} = \frac{\lambda_{d,q}}{i_{d,q}} \quad (3.8)$$

Where $i_{d,q}$ is the winding current and $\lambda_{d,q}$ is the air gap flux linkage in d- and q-axis respectively.

3.4 Start-up

As seen from the rotor design in Figure 3.3a there is no net torque on a locked rotor. Consequently the SynRM is not able to line-start. Instead, a converter is starting and operating the SynRM in variable speed drive (VSD). When the motor is running there are various control techniques to achieve an optimal working point. Some common techniques are Maximum Torque per Ampere (MTPA), Maximum Power Factor (MPF), Maximum Efficiency (ME), Maximum Torque per kVA (MTPkVA) [10]. The drawback of using a converter is additional losses, extra cost and less robustness of the system.

3.5 Efficiency

The efficiency when running in steady-state is one of the main advantages of the SynRM. Since there is no induced current in the rotor the ohmic losses will be small in comparison with the IM. For a 50 Hz 20 kW motor the loss reduction is in the range of 10-30 % and besides the decrease in energy consumption the heat generated in the rotor is also decreased [11]. The SynRM also has the benefit of good air cooling properties of the rotor and does not need any fan in order to cool the rotor.

4

Hybrid rotor modelling

4.1 Hybrid concept

In some applications, such as fan or pump loads, high efficiency is usually the preferred property. In such applications it is interesting with an asynchronous start of the SynRM to avoid the cost of any starting device. By adding a squirrel cage in the rotor this could be achieved. To keep the high efficiency and torque density of the SynRM the squirrel cage should be placed inside the air barriers of the SynRM rotor. This is to avoid disturbing the salience ratio and the iron flux paths.

The equivalent circuit of this hybrid arrangement is somewhat a combination of the IM and SynRM which were described in Figure 2.1 and Figure 3.2. The equivalent circuit of hybrid line-start motor can be seen in Figure 4.1

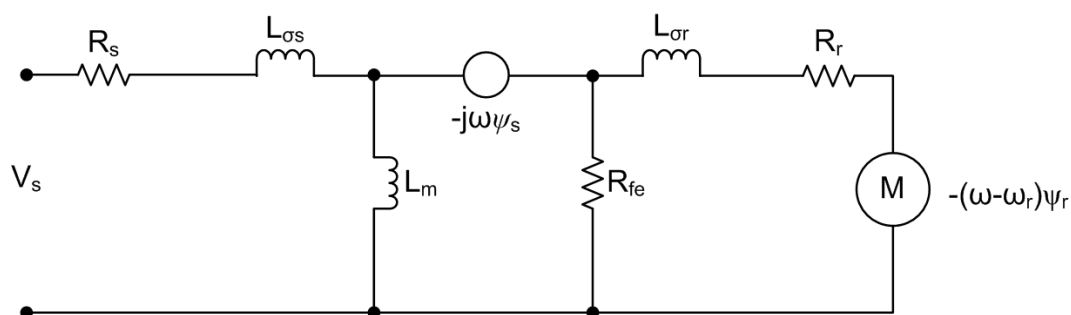


Figure 4.1: Equivalent scheme for the hybrid motor

From a starting perspective this hybrid arrangement will act as an IM with moving torque applied by induced current. However, the salient rotor will, depending on the position, either counteract or increase the moving torque with a reluctance torque. The torque curve for different operating speeds of the hybrid arrangement consists of an asynchronous part (solid) and a reluctance band (dashed lines). The total torque will oscillate within the band during start up.

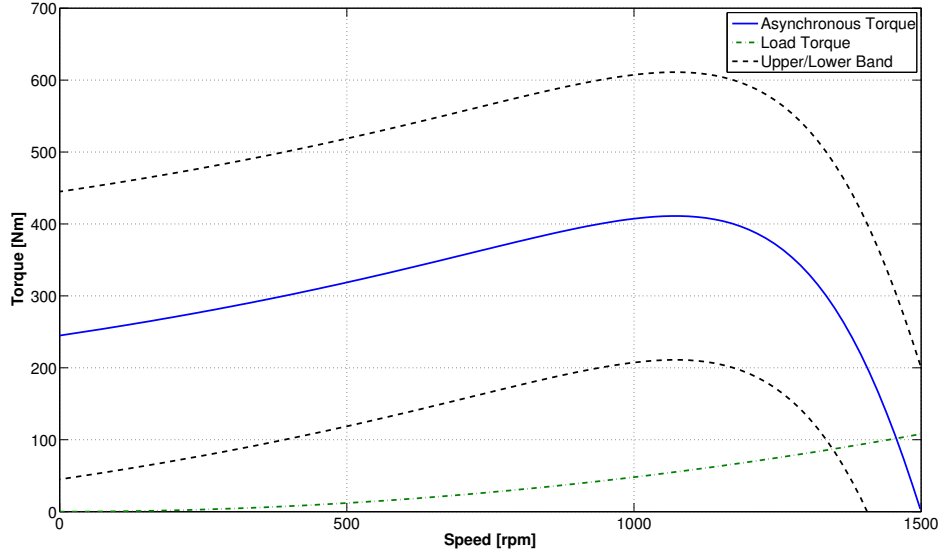


Figure 4.2: Starting torque consist of asynchronous torque from the squirrel cage and a reluctance torque band from the SynRM part

4.2 Simulation setup

To validate the simulation results an existing IM is first modelled and the performance from the simulation and the existing is compared and fine tuned. The limited data for detailed design specifications on existing IM's leaves room for improvements in this model. However, for the sake of comparison the model is deemed to be suitable.

Table 4.1 lists the nominal values for the simulations on the hybrid motor. The friction and windage losses are estimated values in steady state operation and the damping is considered as an extra load torque. From (4.1) the term $B\omega$ is bundled with T_l' into T_l . This means that T_l will have both a quadratic and a linear part.

Table 4.1: Nominal values

Parameter	Value
Power output, P_{out} [kW]	20.0
Speed, n [rpm]	1500
Nominal load torque, T_l [Nm]	122
Inertia, J [kg · m ²]	0.113283
Damping, B [Nm · s/rad]	0.0128045
Friction and windage losses, IM [W]	100
Friction and windage losses, SynRM [W]	100

$$\begin{aligned}
T_e - T_l' &= J \frac{d\omega}{dt} + B\omega \\
T_e - T_l &= J \frac{d\omega}{dt}
\end{aligned} \tag{4.1}$$

The output power and furthermore the efficiency is then calculated from (4.2).

$$\begin{aligned}
P_{out} &= P_{in} - P_{loss,EM} - P_{loss,mech} \\
\eta &= 1 - \frac{P_{loss,tot}}{P_{in}}
\end{aligned} \tag{4.2}$$

4.2.1 Rotor parameters

To evaluate a good design for the hybrid arrangement a parameter study is carried out. In Figure 4.3 the different parameters and their representation is illustrated. The initial motor parameters is presented in Table 4.2. Another parameter, not shown in Figure 4.3 is the shape of the barriers. The shape studied in this thesis is the hyperbolic curve and hyperbolic line, these are shown in Figure 4.4

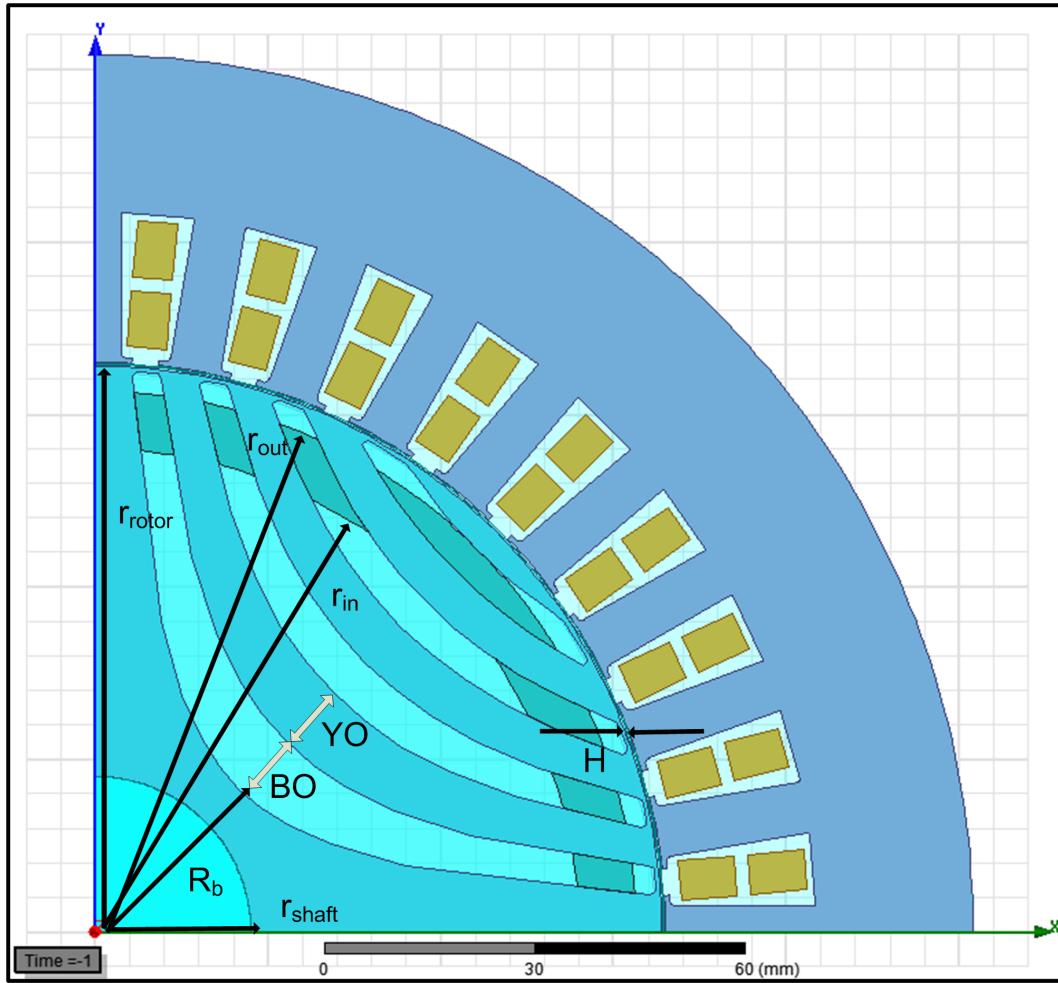
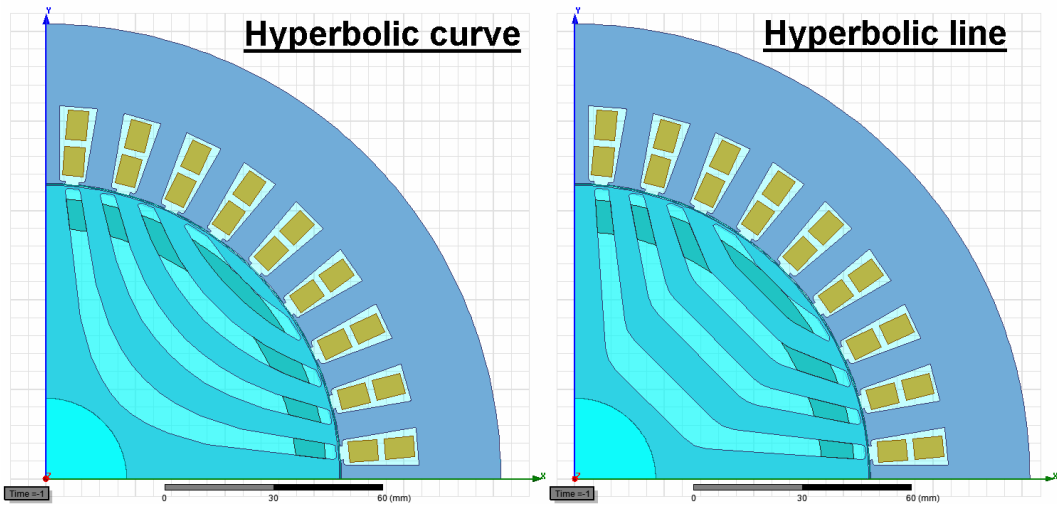


Figure 4.3: Definition of the parameters in table 4.2.

Table 4.2: Initial rotor parameters

Motor parameter	Value
Outer diameter, $r_{rotor}[mm]$	163.9
Shaft diameter, $r_{shaft}[mm]$	45
Number of barriers, k	4
Bottom barrier radius, $Rb[mm]$	29.35
Bottom barrier thickness, $B0[mm]$	9.6
Bottom yoke thickness, $Y0[mm]$	9.825
Bridge thickness, $H[mm]$	0.5
Aluminum outer radius, $r_{in}[mm]$	78.25
Aluminum inner radius $r_{out}[mm]$	70
Barrier shape	Hyperbolic curve

**Figure 4.4:** Comparison of hyperbolic curve (left) and hyperbolic line line geometry (right).

Each barrier shape can also have a cut-off structure which means that the outer part of iron in the q-axis is removed. This structure will not be covered in this section since it will be difficult to implement this with aluminum filling practically. The cut-off structure is briefly mentioned in Section 3.3.1 and further evaluated in [10],[12].

Table 4.3: Different solution methods

Solution type	Industrial analytical model	Thesis analytical model	Thesis FEM model
Frequency [Hz]	67	67	67
Speed [rpm]	1978	1978	1977
P_{out} [kW]	20.0	20.0	20.0
T_n [Nm]	96.6	96.8	96.7
PF	0.81	0.84	0.84
Efficiency	93.0	93.0	93.5
I_n [A]	38.3	36.4	37.7

4.3 Verification

To verify that the model is accurate and no major errors is present a comparison with an existing motor is made. Performance data on an industrial IM was acquired and redesigned with an analytical software. When the performance is similar a FEM model is extracted from the analytical software into a FEM simulation program. Here the design was again analyzed and compared to validate the reliability of the model. It can be noticed that there is a small difference in the solution methods for the same motor and this must be taken into account when analysing the results, see Table 4.3.

Any design changes and analysis is done in the FEM software. For the hybrid motor designs only the rotor is changed from the initial verified IM in Table 4.3

4.3.1 Meshing

To evaluate the influence of the meshing, the coarse and fine mesh are compared to the standard mesh. The most critical areas are the edges of the rotor bars as well as the circumference of the rotor and the air gap. Since the gradient of the magnetic flux is large in the air gap it is important to have a sufficiently good mesh. To take this into account an extra layer is added in the air gap. A plot of the mesh in the air gap is shown in Figure 4.5.

In the rotor bars the influence of the skin depth needs to be taken into account of too. In Figure 4.6 it is shown that harmonics of 1800 Hz are dominating. In order to be able to catch the higher order of harmonics both the mesh and time step needs to be refined.

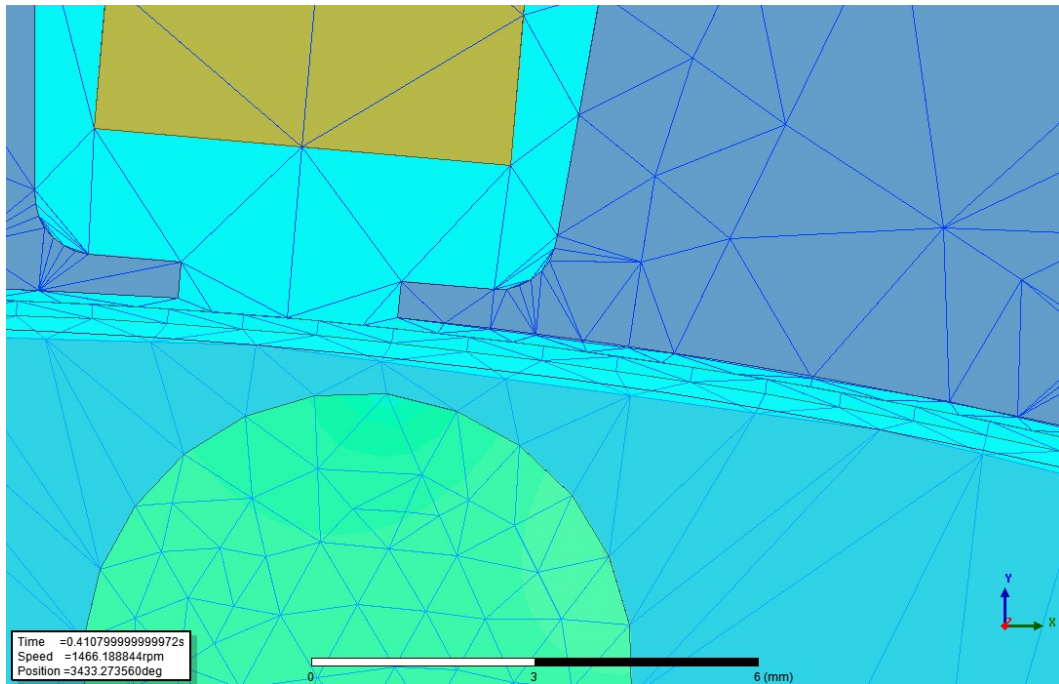


Figure 4.5: Three layers of mesh in the air gap due to the high gradient of the field.

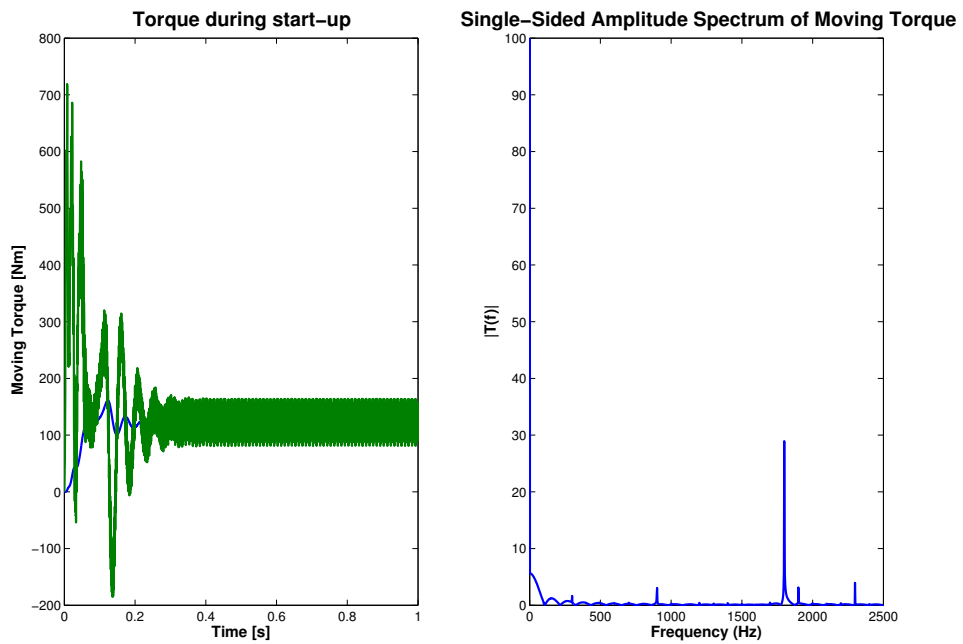


Figure 4.6: Torque ripple (left) and Fourier analysis of the torque ripple (left).

The skin depth of the 1800 Hz harmonics in aluminum is about 2.5 mm. The effect of skin depth is illustrated in Figure 4.7 and is described by (4.3).

To be able to catch the influence of the 1800 Hz harmonic a mesh containing at least 2 elements wide must be contained within the aluminum. In the stator core and windings the mesh is presumed sufficient at standard settings.

$$\delta(f) = \sqrt{\frac{\rho_{al}}{f\pi\mu_{al}}} \quad (4.3)$$

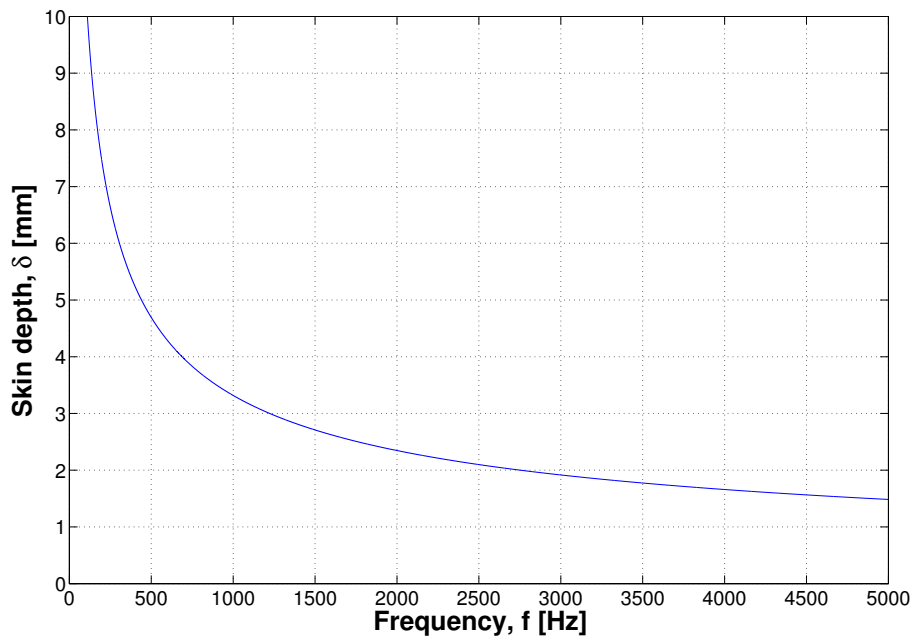


Figure 4.7: Skin depth for different frequencies in aluminum.

4.3.2 Time step

Having a sufficient time step in a simulation is important. Having a too short time step will increase the simulation time however, having a too long time step can neglect important harmonics. To find the interesting time step for the simulation one must have knowledge about what harmonics is in the model simulated. The harmonics that have notable influence are in the range of 1800 - 3600 Hz. To capture the 3600 Hz component as good as possible without extensive simulation times, 6-8 samples per period is deemed to be sufficient.

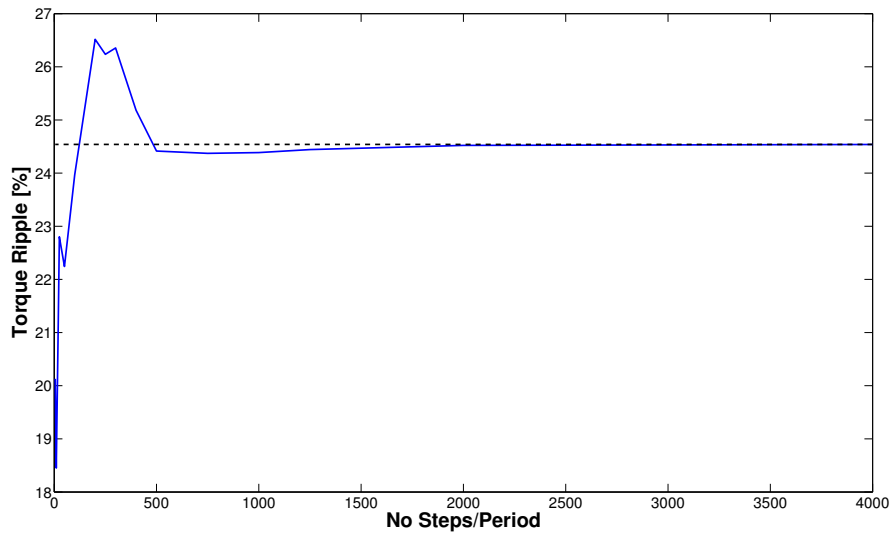


Figure 4.8: Torque ripple in percent of nominal torque vs. the number of time steps per period.

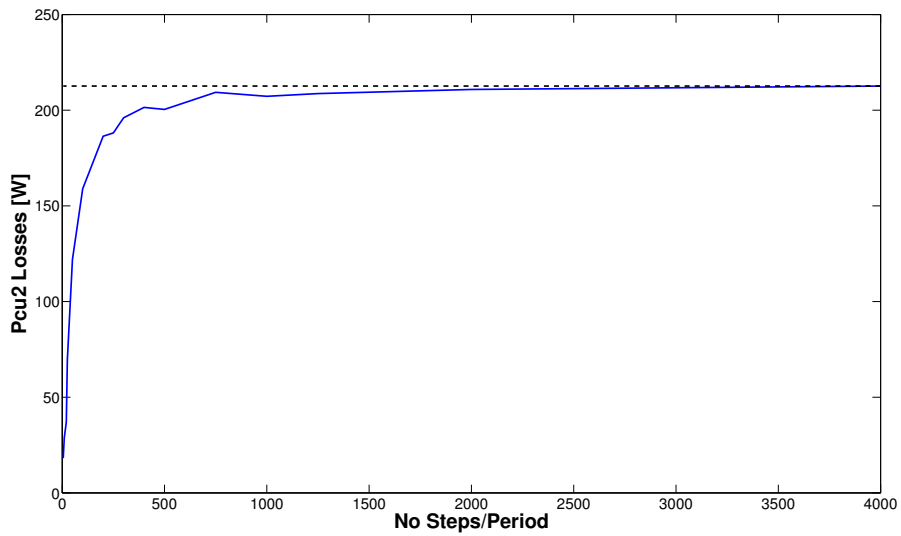


Figure 4.9: Losses in rotor bars vs. the number of time steps per period.

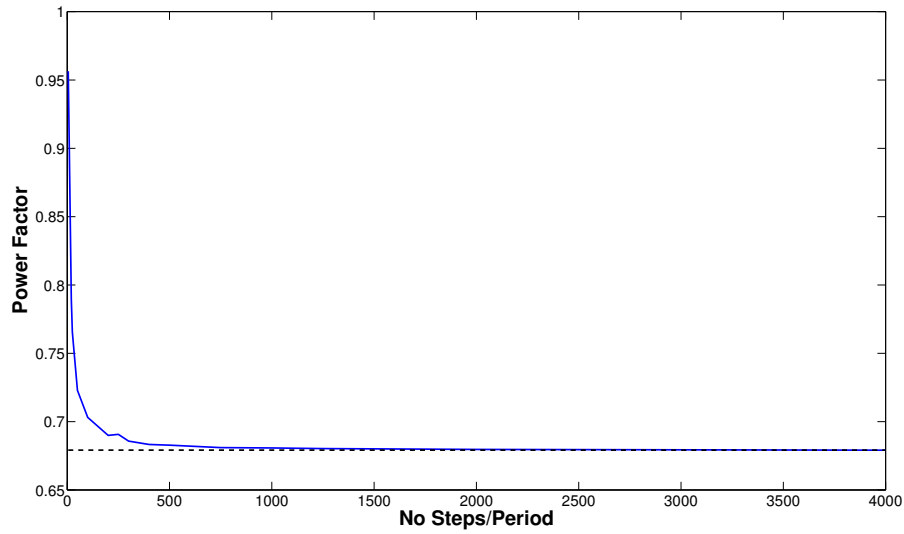


Figure 4.10: Power factor vs. the number of time steps per period.

As can be seen from Figure 4.8-4.10 at 500 steps per period the curves begins to converge. However, the losses still seemed to increase beyond 4000 steps and to get accurate final values a finer time step might be needed. There is a slight peak in the torque ripple around 200 - 400 time steps per period but at 500 samples per period this peak is avoided. The power factor is sensitive to having too few time steps but it saturates at about 500 time steps per period.

5

Simulation results

In this chapter a study of the hybrid line start motor is carried out by FEM simulations. The results are presented from both start up and steady state perspective. The motor model presented in the Chapter 4 will act as a reference when different parameters in the rotor are changed or swept in order to see how these changes affect the performance.

To limit the computational time a 2D axis-symmetrical geometry was used and the maximum number of elements was varied depending on what physics that was investigated. The mesh used contained roughly 10000 elements for a quarter of the motor. To capture dynamics during start-up 500 samples per period was used throughout the simulations.

5.1 Start-up

It is considered acceptable if the motor is able to synchronize at nominal torque, -inertia and -damping. When the rotor is at zero or low speed the asynchronous torque will be dominating but when synchronized harmonics will induce currents in the rotor and give rise to additional losses.

To get a brief perception on the starting ability an initial model is evaluated. The run up characteristic is shown in Figure 5.1. As can be seen there is a speed dip at around 1200 rpm. This dip occurs due to that the reluctance torque has greater influence and is opposite to the asynchronous torque. Depending on the starting position of the rotor and rotor parameters the speed dip occurs at different instances.

To evaluate the starting performance a starting time is defined. The starting time, t_{start}

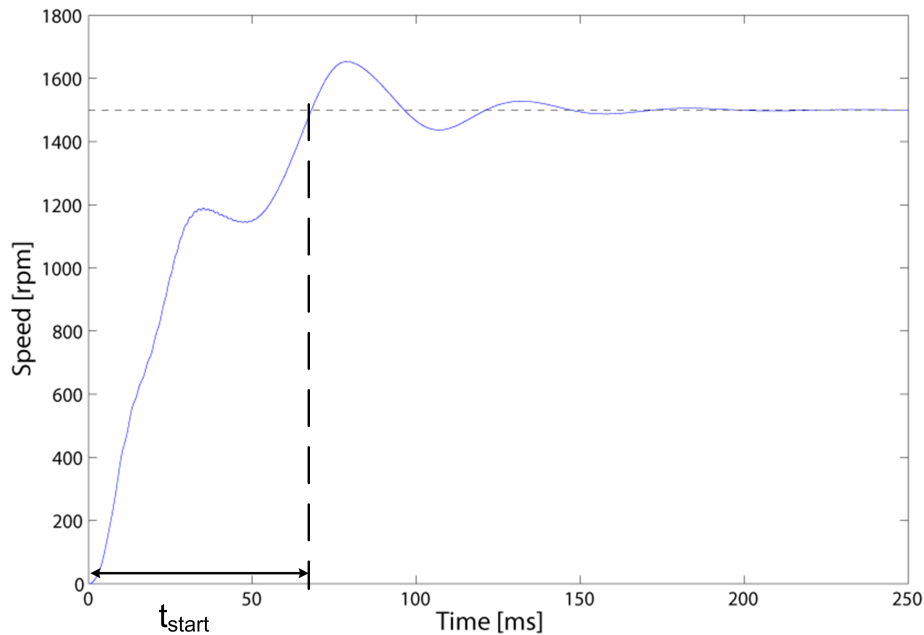


Figure 5.1: Starting time

is the time from zero to synchronous speed and is illustrated in Figure 5.1. For the initial motor design $t_{start} = 67.5$ ms.

If the load torque is higher than the pull in torque the motor will not synchronize but instead start oscillating with high slip. An example of this is shown in Figure 5.2.

Number of barriers

The number of barriers will have a direct influence on the width of the aluminum bars in the rotor. This parameter will have a great impact on the starting strength of the motor. The size of the aluminum bars determine how much current that will be induced during start up and consequently the start up torque.

The barrier thickness also affects the reluctance which has a large impact on starting time and steady state performance. Because of this there are many aspects involved by changing this parameter. As seen in Figure 5.3 there is a non-linear relation of how the motor is being pulled in to synchronous speed. The starting time for the different number of barriers is presented in Table 5.1

By studying the torque during start up it can be concluded that 4 and 6 barriers has

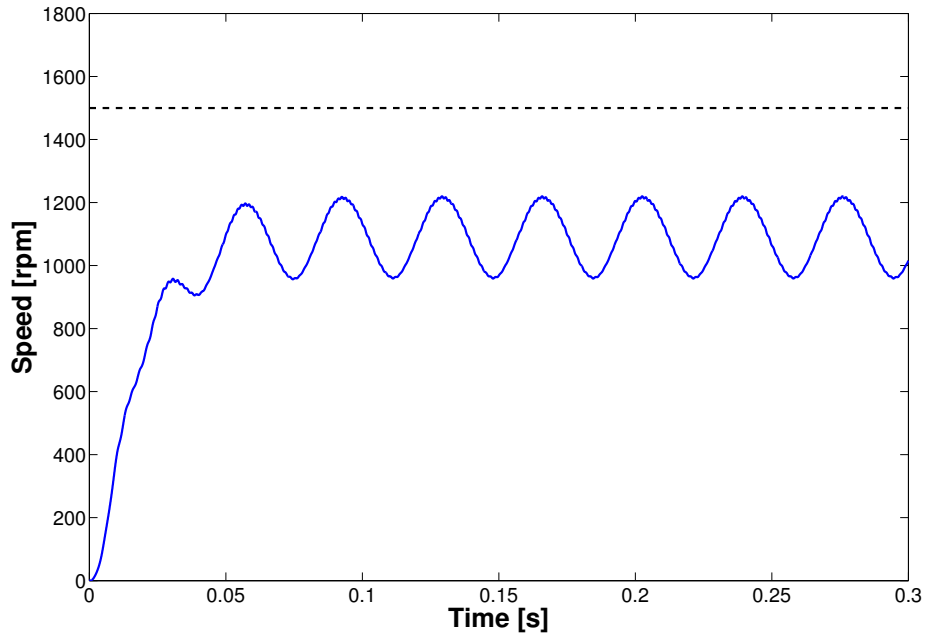


Figure 5.2: Speed characteristic when the motor is not able to synchronize (500 % nominal load torque).

Table 5.1: Starting time for different number of barriers

Number of barriers, k	Starting time [ms]
4	67.5
5	69.6
6	58.6

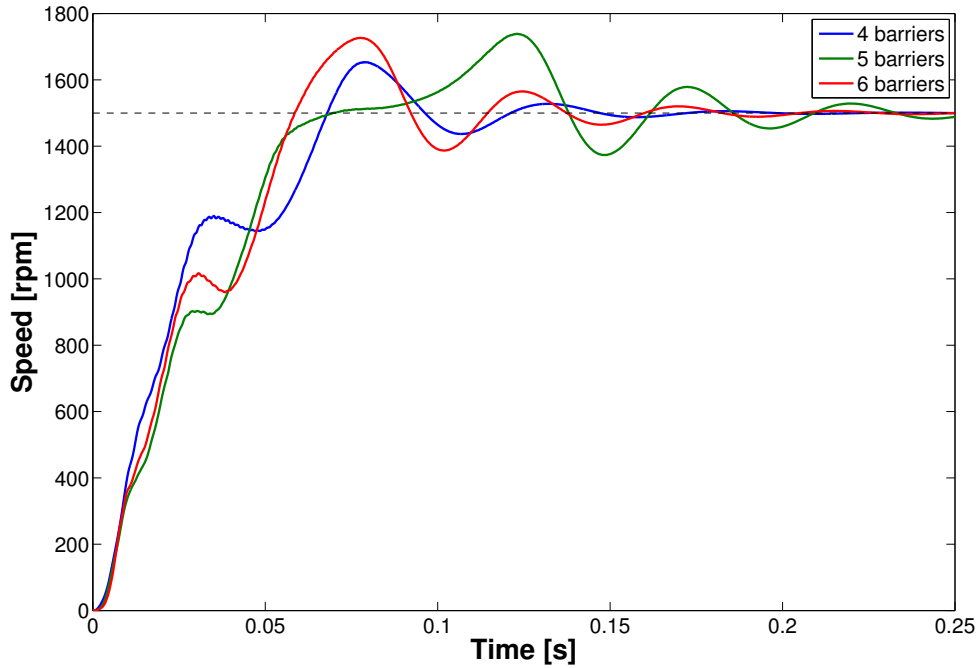


Figure 5.3: Speed curves for different number of barriers during start-up of the motor (same starting position).

a smoother torque transient comparing to 5 barriers. For a 4 barrier rotor the torque ripple is significantly lower as well. This is illustrated in Figure 5.4 and further presented in Section 5.2.

Barrier shape

The comparison between the different barrier types in Figure 4.4 gave a similar result, as seen in Figure 5.6.

However, the difference between the barrier types becomes more distinct when the aluminum filling is increased. In Figure 5.7 the barriers are completely filled and the hyperbolic curve has a much lower starting time.

Another option concerning the barrier shape is to remove the end bridges in order to induce more current in the rotor bars and increase the saliency ratio. In Figure 5.8 this comparison is plotted. There is not much difference in the starting time compared to the initial design.

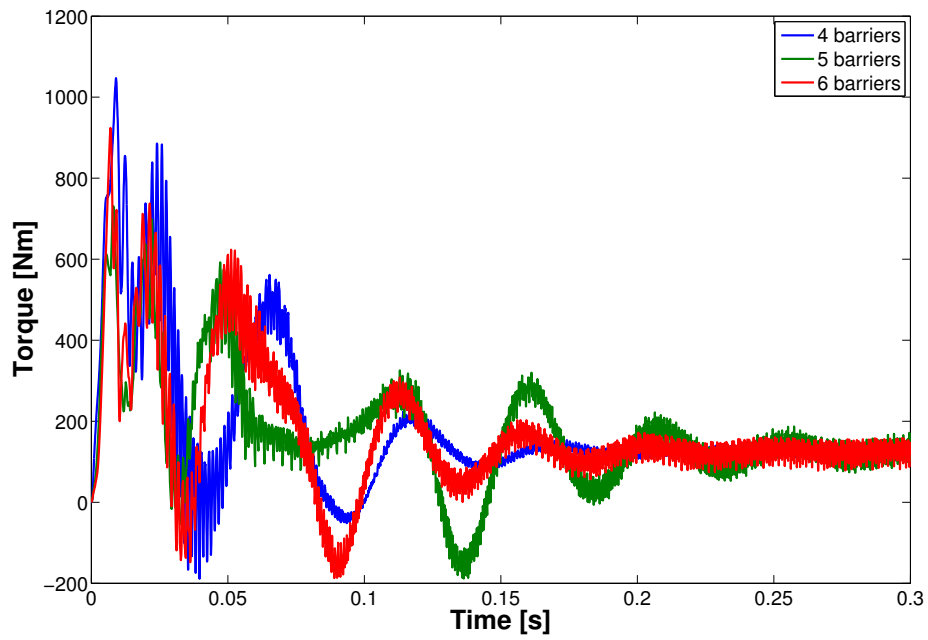


Figure 5.4: Torque curves for different number of barriers during start-up of the motor (same starting position).

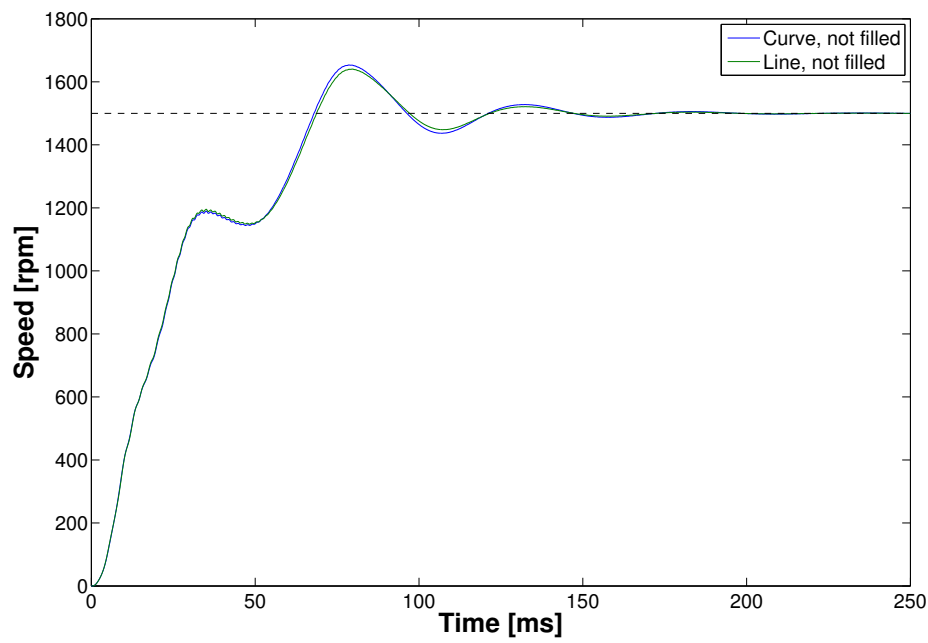


Figure 5.5: Curve and line comparison.

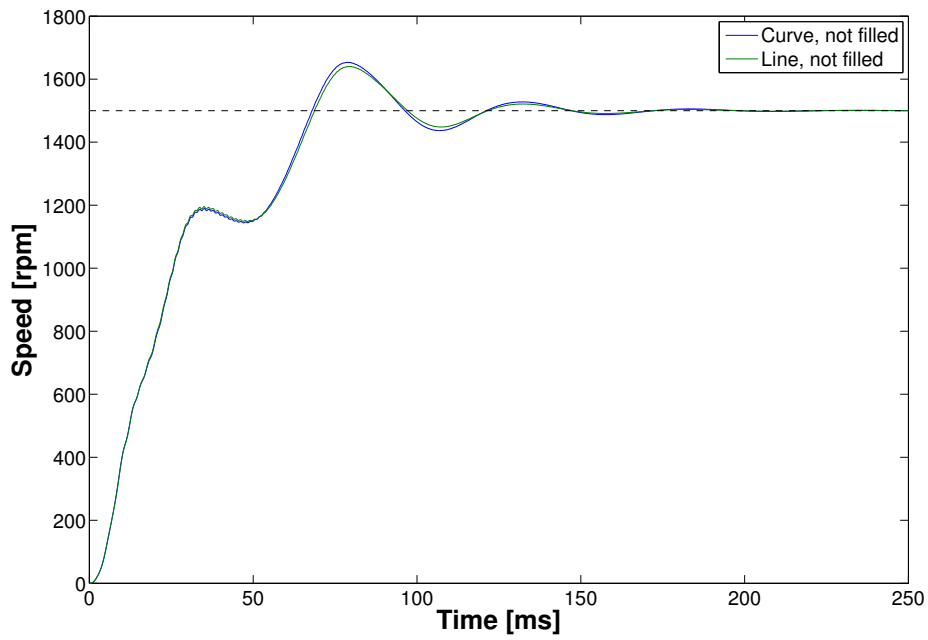


Figure 5.6: Hyperbolic curve and hyperbolic line comparison when the barriers are partly filled by the cage.

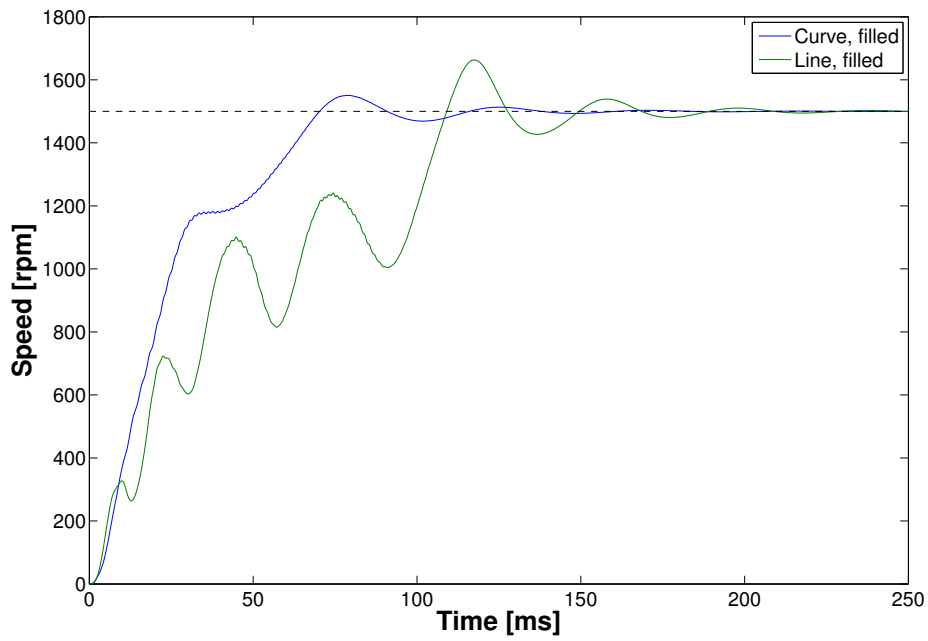


Figure 5.7: Curve and line comparison, barriers completely filled.

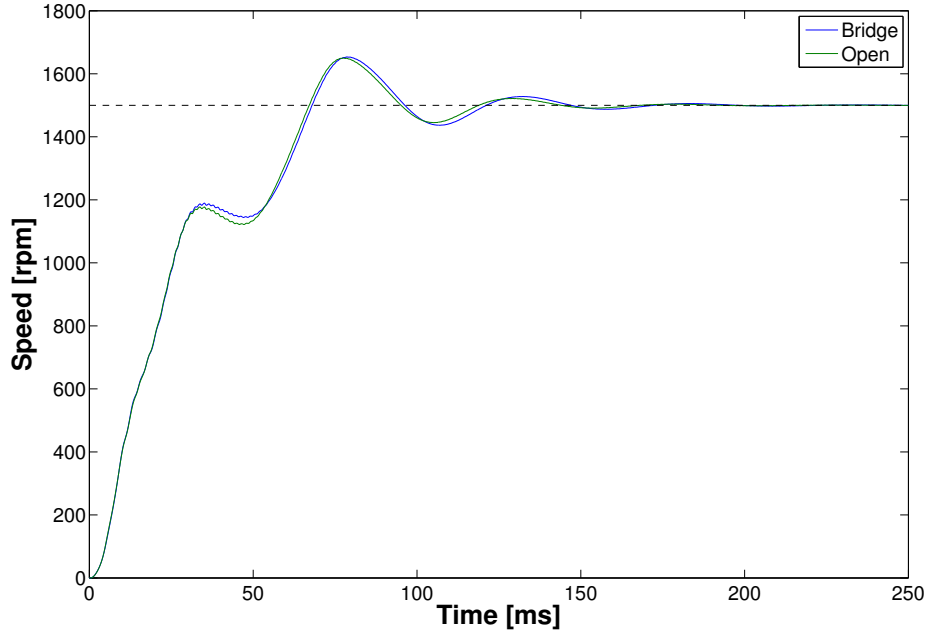


Figure 5.8: The rotor with no end bridges for partly filled, hyperbolic curve barriers (Hybrid 1).

Barrier filling at start up

As seen in Figure 5.9 the current density is higher at the outer part of the rotor and close to zero towards the middle. Hence, the aluminum in the middle has no or little impact on the starting torque of the motor. A parametric study is made to further confirm that the aluminum closest to the shaft has no or little influence of the performance. As can be seen in Figure 5.10 the start of the motor is almost unchanged from $r_{in} = 0$ mm to $r_{in} = 70$ mm. The starting torque of the motor slightly increases when increasing r_{in} , see Figure 5.11 and Figure 5.13. This is due to that the current is localized where the generated torque has the most effect i.e. at the circumference of the rotor.

It can be seen by Figure 5.12 that the changes in P_{cu2} losses is neglectable when changing R_{in} .

Extra coil in rotor along d-axis

To evaluate the influence of an extra conductor in the d-axis the design in Figure 5.14 is simulated. From the speed plot of the start in Figure 5.15 it can be concluded that this idea is not good from a starting point of view. The starting time for this design is

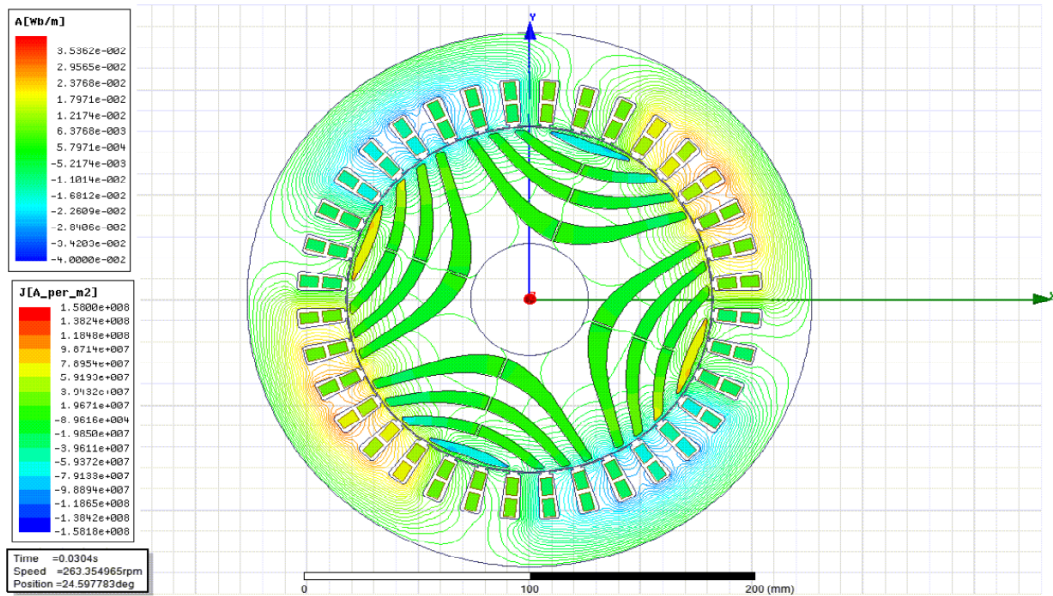


Figure 5.9: Current density and field lines during start up when the air barriers are completely filled with aluminium (Initial design).

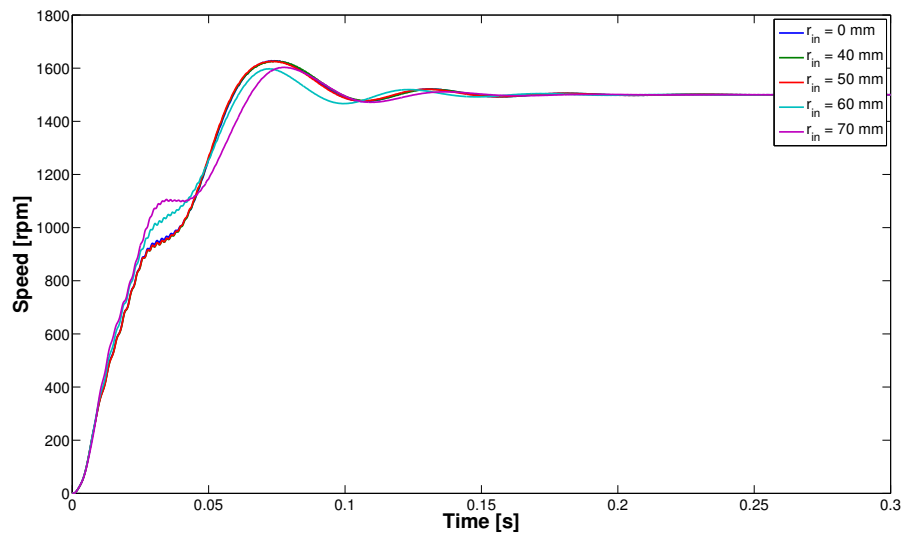


Figure 5.10: Run-up characteristic for different aluminum inner position (r_{in}).

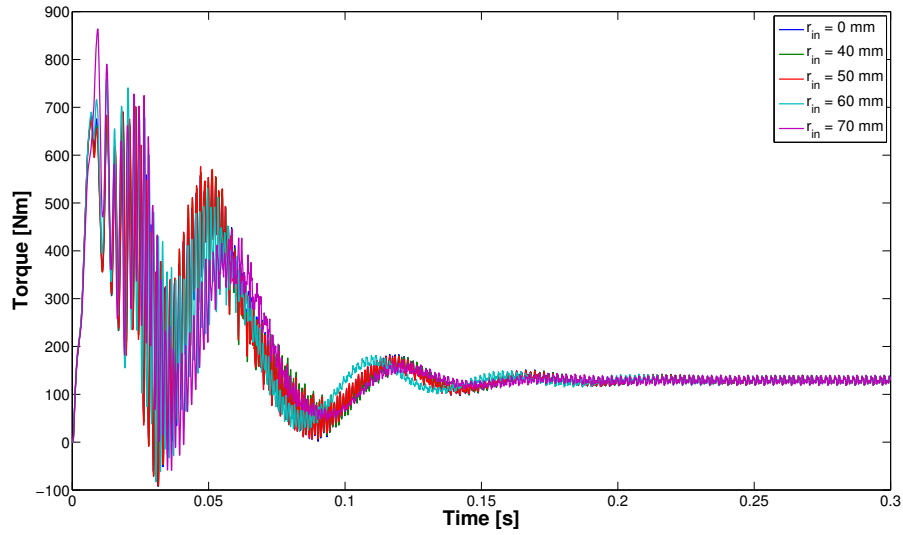


Figure 5.11: Starting torque over time during start transient for different aluminum inner position (r_{in}).

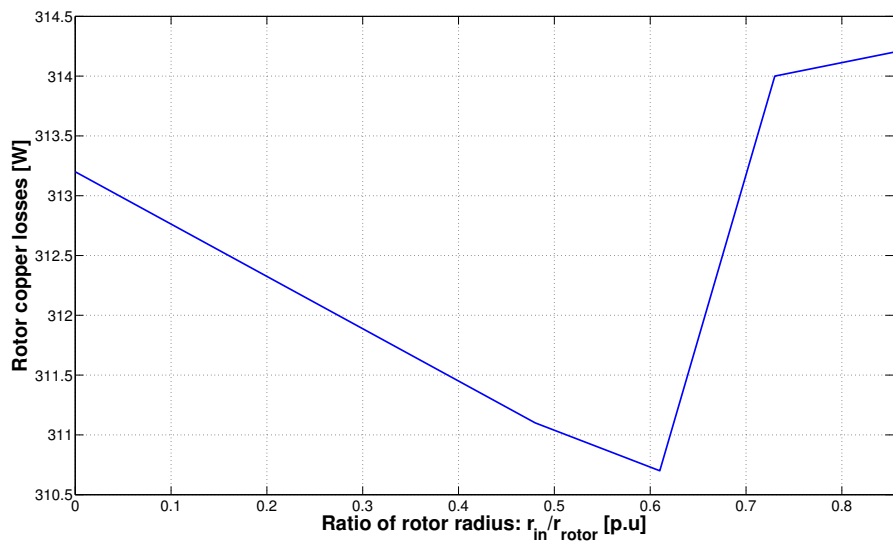


Figure 5.12: Rotor copper losses as a function of cage inner radius R_{in} placement.

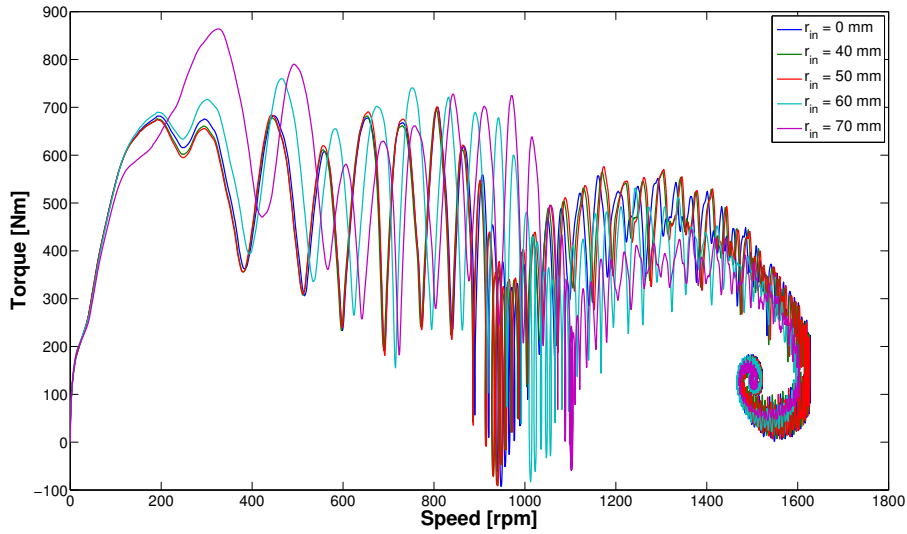


Figure 5.13: Starting torque against speed for different aluminum inner position (r_{in}).

$t_{start} = 101.4$ ms in comparison to the initial design $t_{start} = 67.5$ ms.

Starting position of rotor

During the start of the hybrid machine the reluctance part will act as an oscillating torque depending on the angular position. It is important to find the position during the start up with the least amount of negative torque to avoid vibrations and mechanical stress.

From Table 5.2 it can be concluded that the starting position has a significant influence on the starting time. From the worst position to the best the starting time is reduced almost 60 %. However, the motor is able to synchronize from all starting positions as shown in Figure 5.16. For positions with longer starting time e.g. $\theta_{start} = 40^\circ$ the mechanical tension is a bit higher. This is shown from the torque characteristic in Figure 5.17.

5.2 Steady state

The steady state performance is the area of interest due to the short start up sequence. The motor will mainly be operating in steady state and the efficiency class is determined by how well the motor performs in steady state operation.

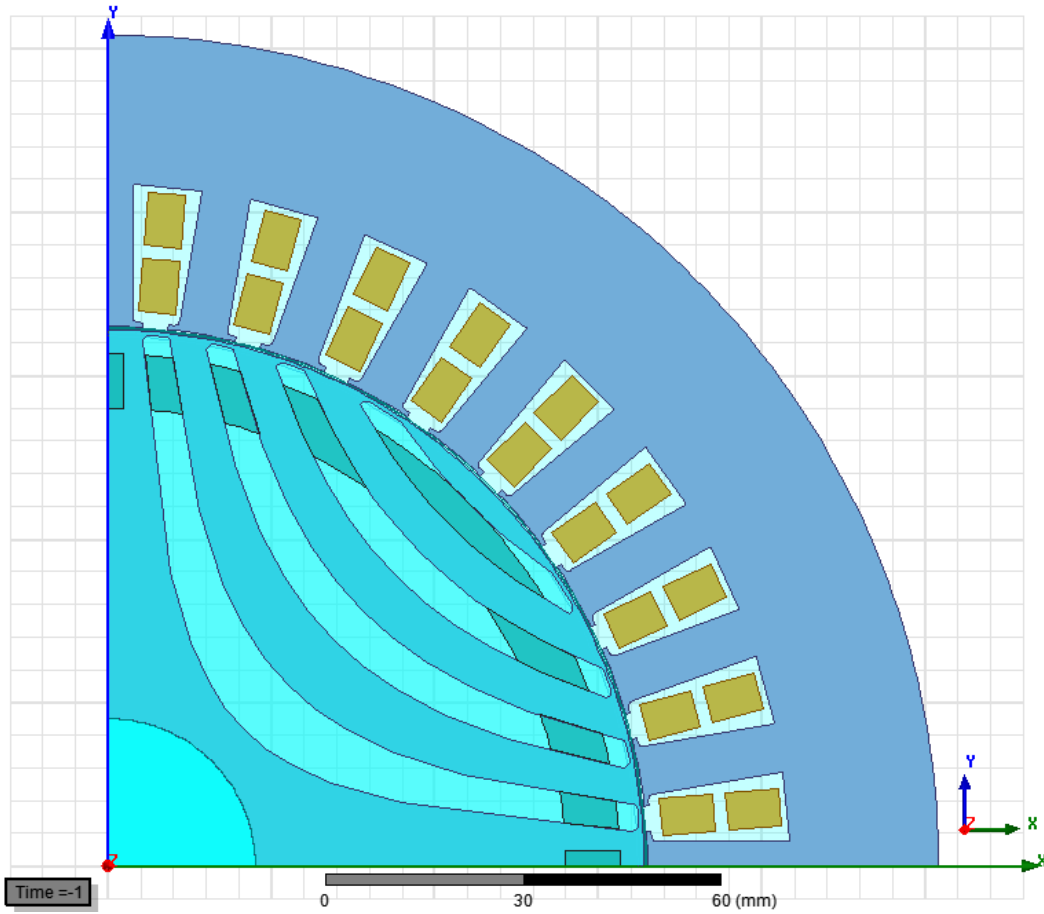


Figure 5.14: Model design for extra conductor in rotor slot d-axis.

Table 5.2: Starting times with different initial positions for the rotor for the initial design

$\theta_{position}$	T_{start}
0°	132.2 [ms]
20°	77.6 [ms]
40°	100.5 [ms]
60°	92.1 [ms]
80°	74.8 [ms]

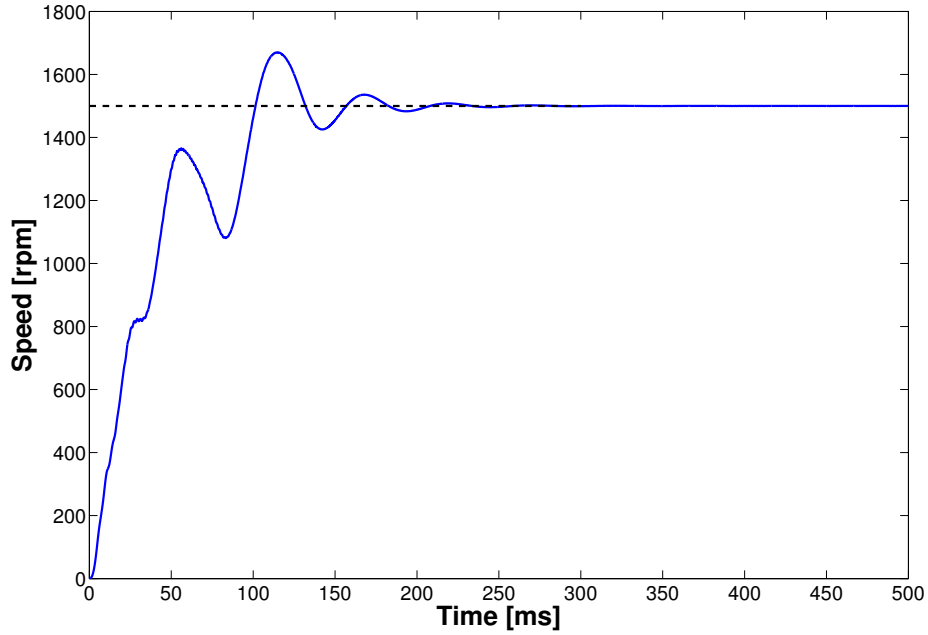


Figure 5.15: Speed characteristic with extra conductor in d-axis.

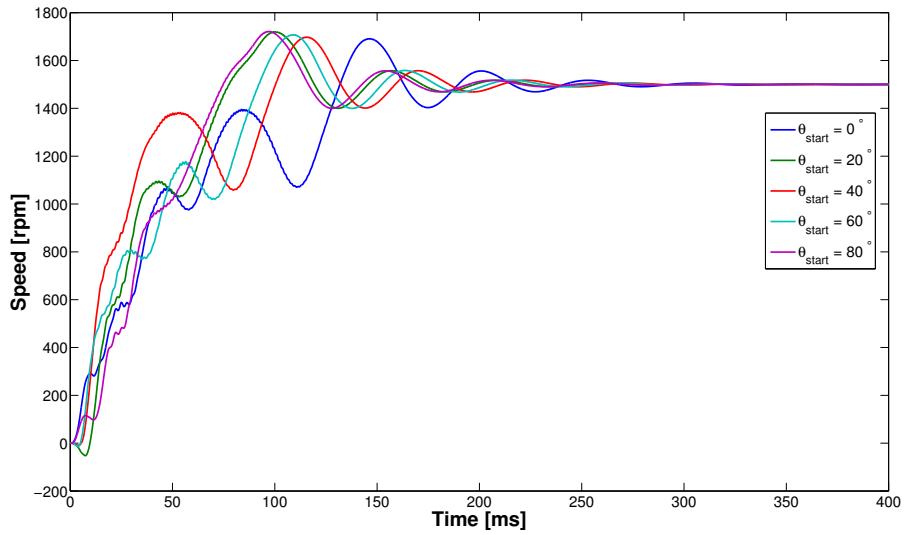


Figure 5.16: Speed, run up characteristics with different starting positions for the rotor.

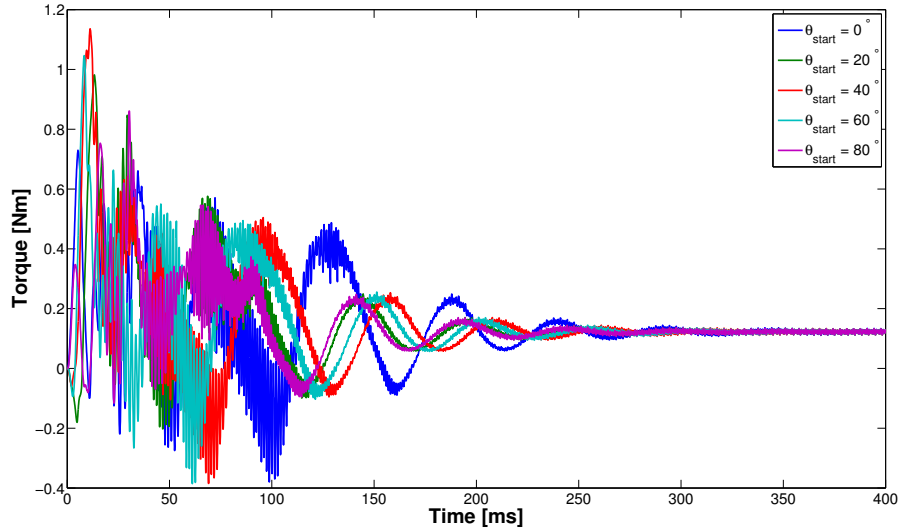


Figure 5.17: Torque characteristics for different starting positions of the rotor.

Table 5.3: Steady state performance with different number of barriers

No. Barriers	PF	P_{cu2} [W]	T_{ripple} [%]	Total Loss [W]
4	0.685	227	23.0	1175
5	0.698	539	55.3	1495
6	0.702	783	45.0	1740

Number of barriers

The steady state performance is investigated with different number of barriers, with the air barriers completely filled with aluminium and with no other optimization and the results can be seen in Table 5.3.

It can be noticed from Table 5.3 that the rotor with 4 barriers has the lowest losses, lowest torque ripple and slightly higher power factor.

Barrier geometry

The variation of Y_0 and B_0 is shown in Figure 4.3 and Table 4.2 and is investigated in relation to torque ripple and efficiency. The results are shown in Figure 5.18 and Figure 5.19. As seen in Figure 5.18 the barrier design has a big impact on the torque ripple of the motor. By adjusting the barrier dimensions by a few millimeters a reduction in

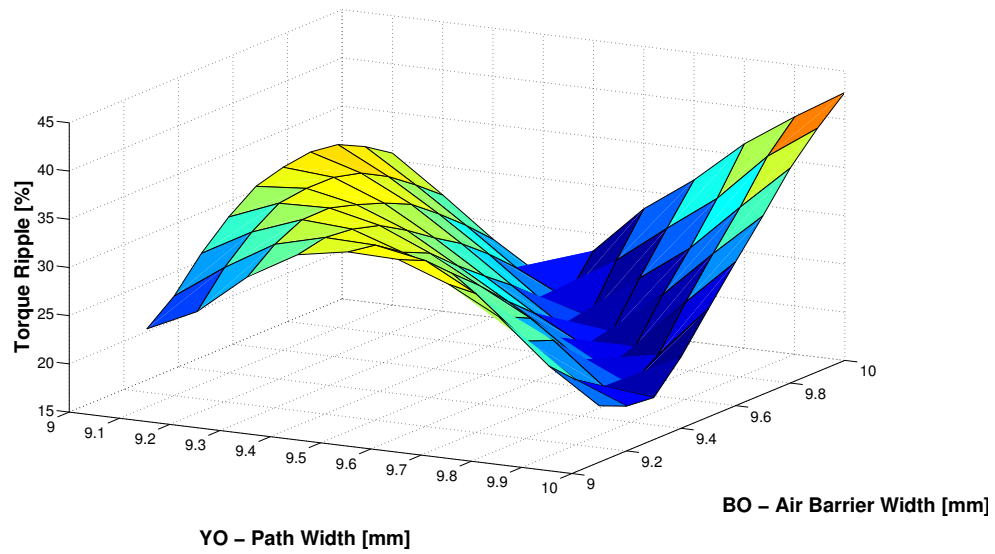


Figure 5.18: Torque ripple for different air-barrier designs.

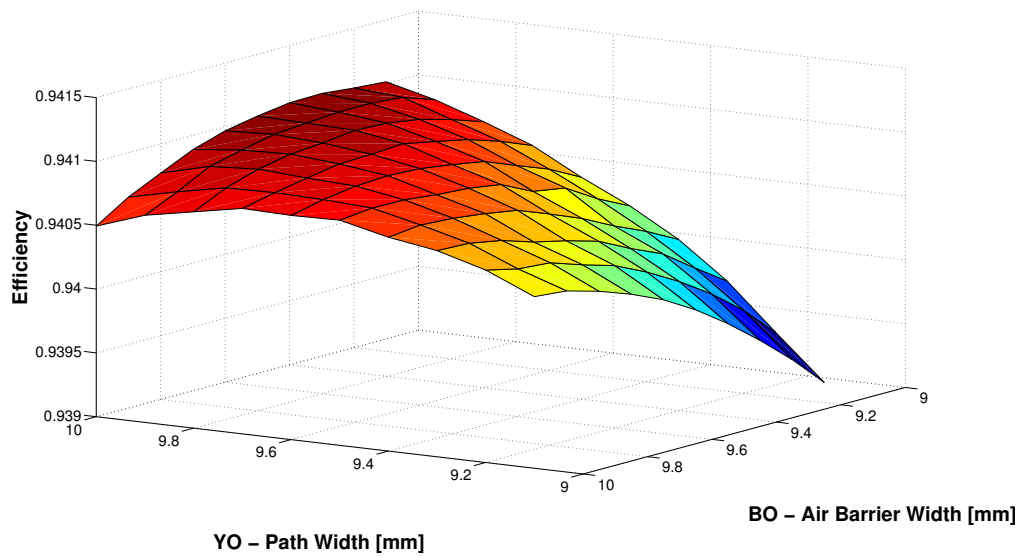


Figure 5.19: Efficiency for different air-barrier designs.

the torque ripple can be made by 50 %. As seen in Figure 5.19 the barrier design has a smaller impact on the efficiency than on the torque ripple of the motor. The efficiency is around 94.0 % in the studied range of YO and B0 while the torque ripple is between 15 and 45 %.

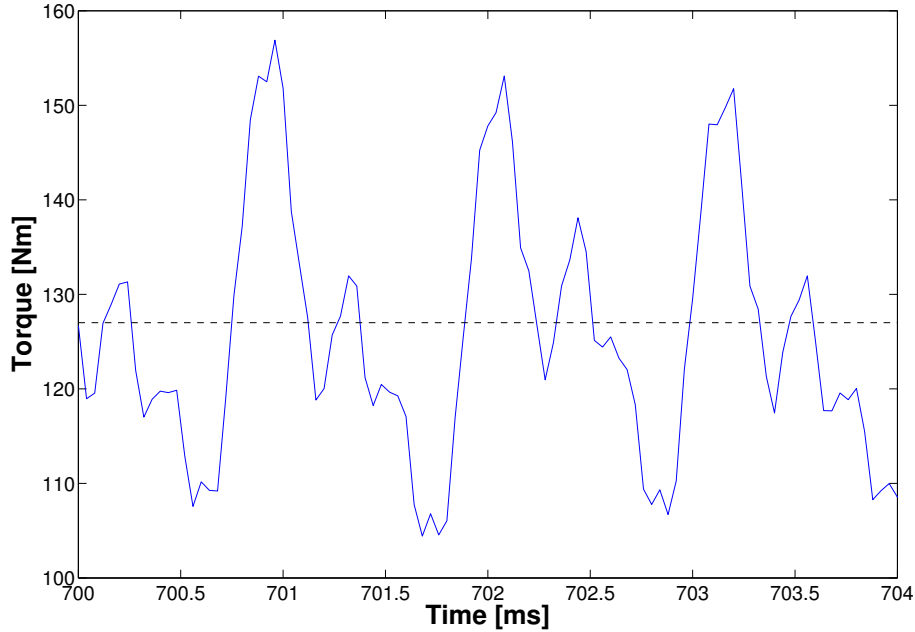


Figure 5.20: Torque ripple is 41.7 % in steady state for open barriers design.

An option investigated for the start up performance was the open barriers, see Figure 5.8. This did almost no difference in starting time. However, in steady state the open barriers had a great influence on the torque ripple in comparison to the closed barriers. In Figure 5.20 it is shown that the torque ripple for the rotor with open barriers is 41.7 % which is more than double of that for the closed barriers.

In Figure 5.21 it can be seen that the P_{cu2} losses increased with open barriers.

Extra conductor in rotor along d-axis

In Section 5.1 the start was simulated with an extra rotor conductor in the d-axis. In Figure 4.6 it was concluded that the stator slots was the main origin of harmonics, the 1800 Hz component. By comparing this with Figure 5.22 this is verified due to the harmonic content in this model. Furthermore, the P_{cu2} losses increases slightly with an added conductor and the power factor increased from 0.707 to 0.727.

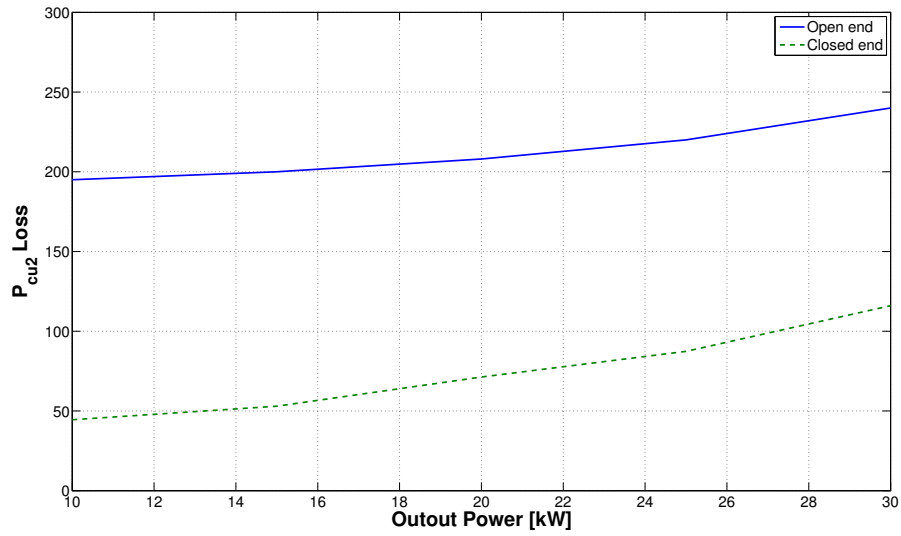


Figure 5.21: Rotor copper losses at different output power for open barriers and closed barriers.

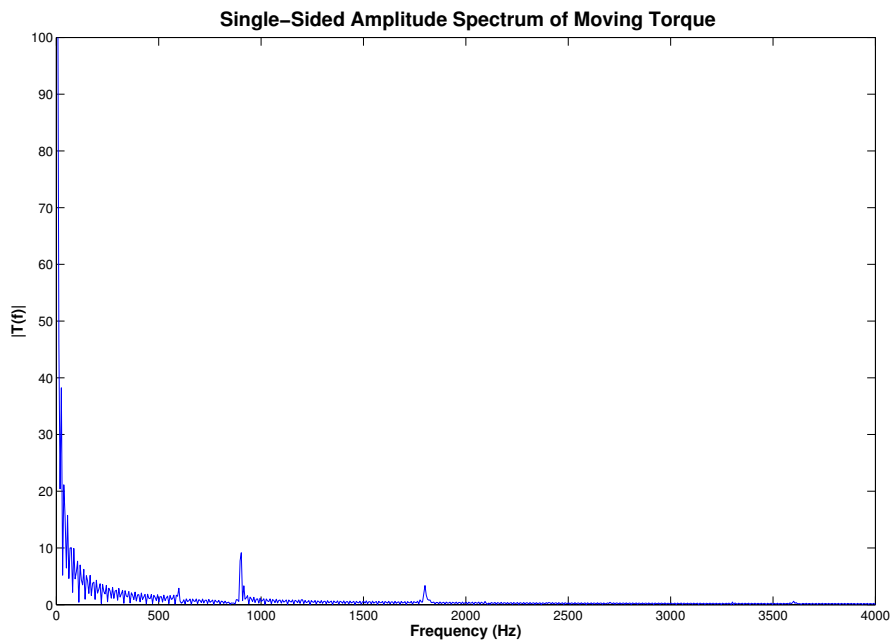


Figure 5.22: FFT of moving torque when an extra coil is inserted in the d-axis.

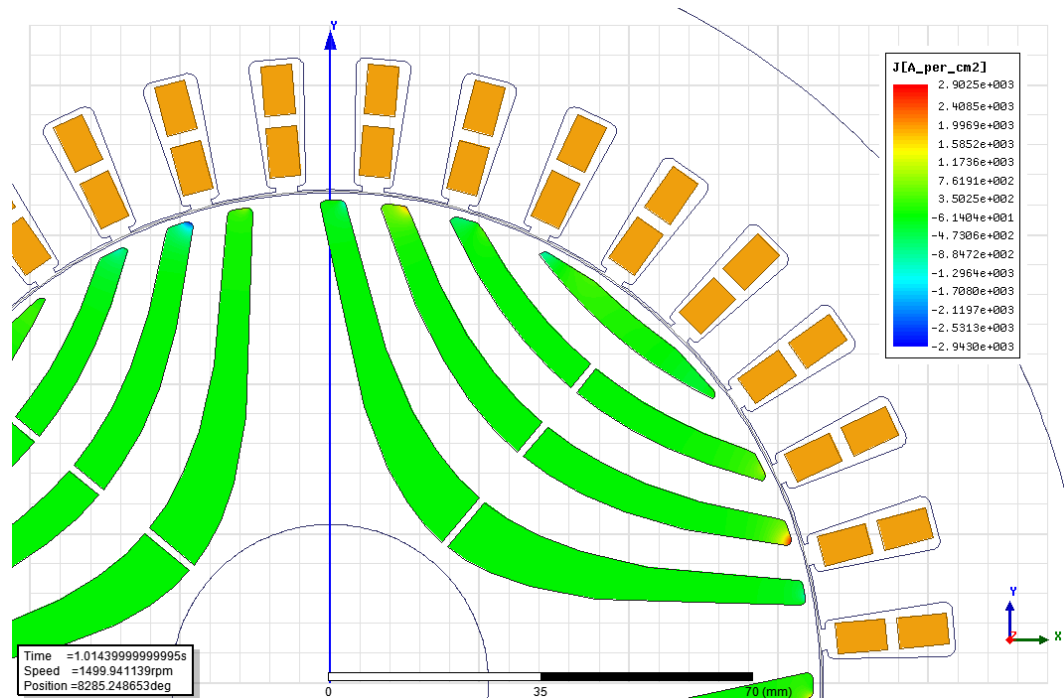


Figure 5.23: Current density in the aluminium bars during steady state.

Barrier Filling in steady state

At synchronous speed there should theoretically be no induced currents in the rotor bars. However, there will always be some harmonics in the air gap that can induce currents at synchronous speed as seen in Figure 5.23. These currents give rise to unwanted losses in the rotor since they produce no active torque and increase the operating temperature of the motor. Limiting these losses is essential for this type of hybrid motor since when compared with an IM this is the area where the greatest loss reduction can be achieved. The induced current might also give rise to torque ripple which is also stressing the motor.

As seen in Figure 5.23 there are currents induced in the outer part of the rotor bars closest to the stator. In steady state these are not wanted and produce no active torque for the motor.

In Figure 5.24 the P_{cu2} losses decrease when the cage outer radius is decreased to the point when the cage becomes too weak to enable synchronization.

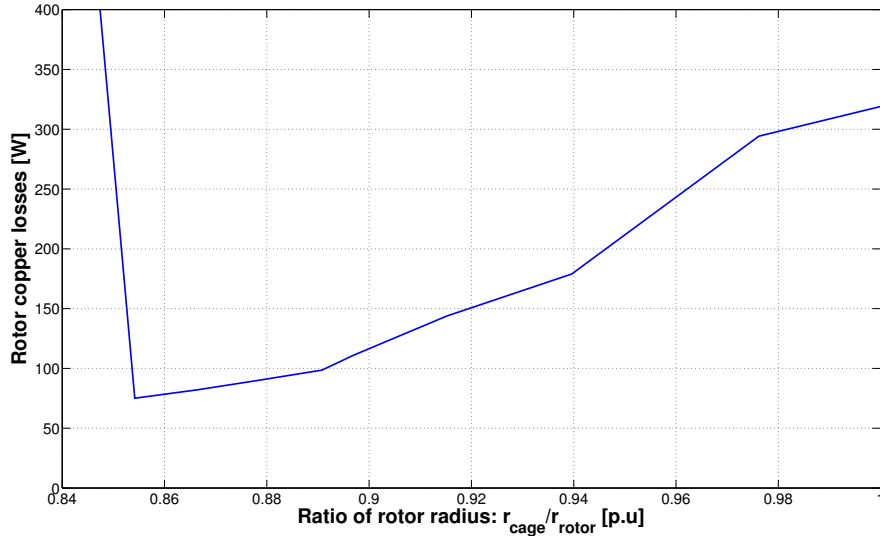


Figure 5.24: Rotor copper losses as a function of cage outer radius placement.

5.3 Promising designs

In this section a combination of the results from the different design variations are taken into account to improve the steady state performance without losing too much of the starting capability.

5.3.1 Hybrid-1, circular cage

From the previous sections it is shown that the model developed from the design in Figure 4.3 has good properties both regarding start and steady state operation. In Figure 5.25 an illustration over the current density induced in the rotor cage during steady state.

5.3.2 Hybrid-2, elliptic cage

In Section 3.3.1 it can be concluded that there is higher MMF close to the shaft of the rotor compared to the perimeter. In the outermost barrier there will be more current induced and thereby more losses. An attempt to decrease the losses but still have good starting performance is introduced by increasing the aluminum filling close to the d-axis of the rotor. This is done by an elliptic cage layout as seen in Figure 5.26. This makes it possible to decrease r_{out} while keeping the starting performance.

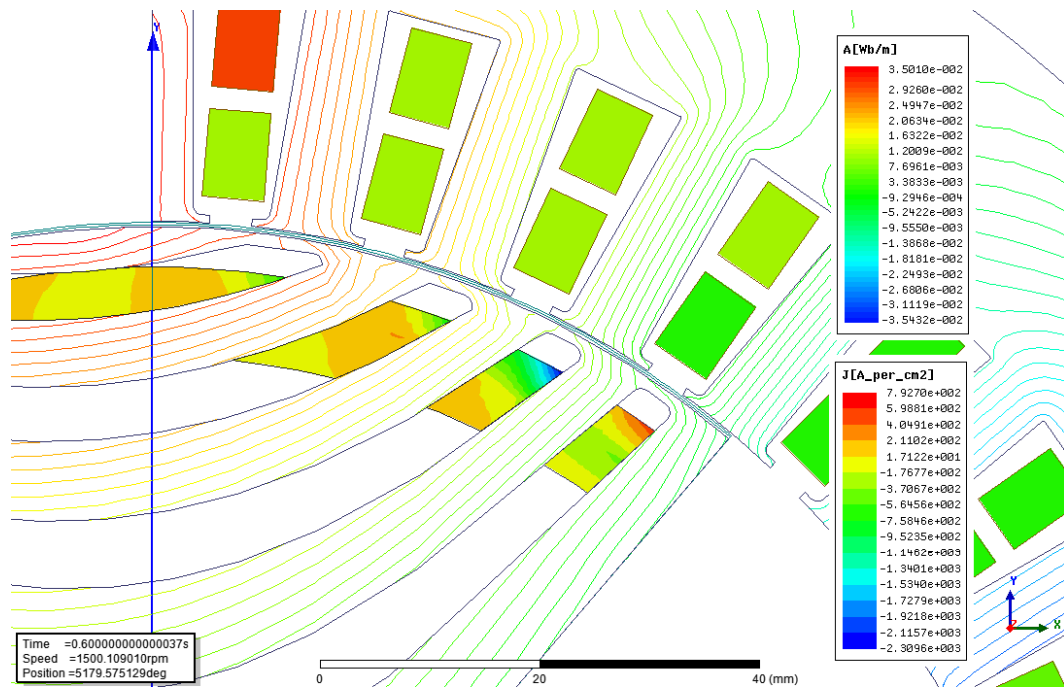


Figure 5.25: Current density and flux lines in the machine Hybrid-1 in steady steady state.

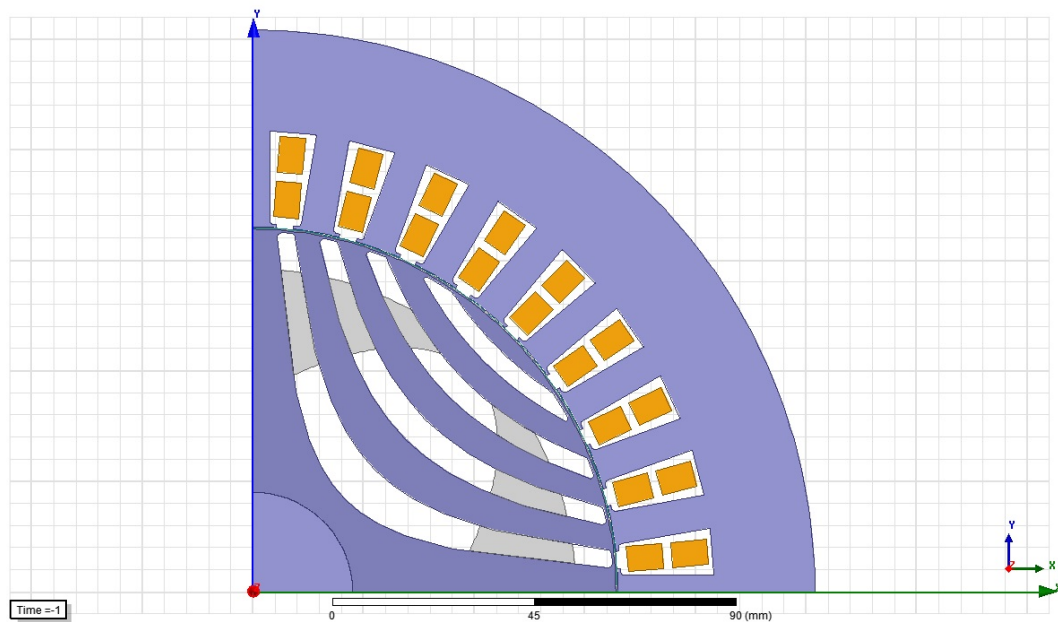


Figure 5.26: Cross section of Hybrid-2 motor design.

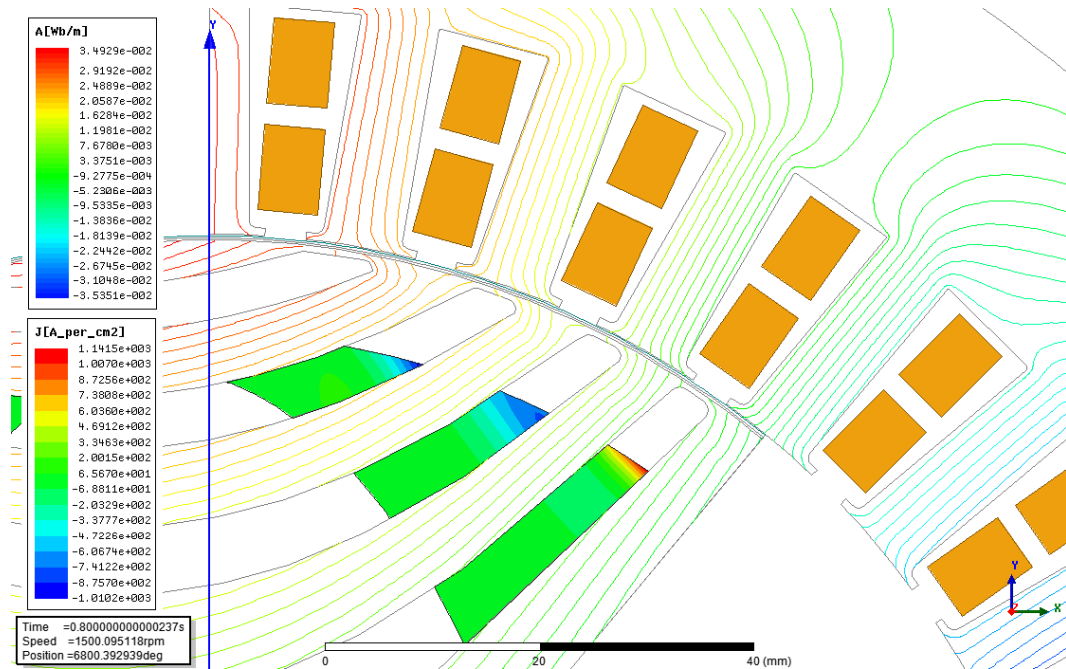


Figure 5.27: Current density and flux lines in the machine Hybrid 2 in steady state.

It can be noticed that in Figure 5.27 the current density has reduced by a factor more than two compared with Figure 5.23. The total rotor copper losses are much lower compared with that for the IM at different power levels (shown in Figure 5.28). Since the other losses are approximately equal the total losses follows the difference for rotor copper losses. The total losses are shown in Figure 5.29.

The power factor for the hybrid motors is slightly lower than the IM but the difference is constant for increasing power.

The rotor cage is also pulled in from the stator to limit the eddy current effect in the bars during steady state and the end bridges of the SynRM structure are kept to further limit eddy currents. Since the inner part of the rotor cage has little or no effect on the starting it is removed to avoid further losses and dead weight. A performance summary of the two models together with the SynRM and IM is presented in Section 5.4.

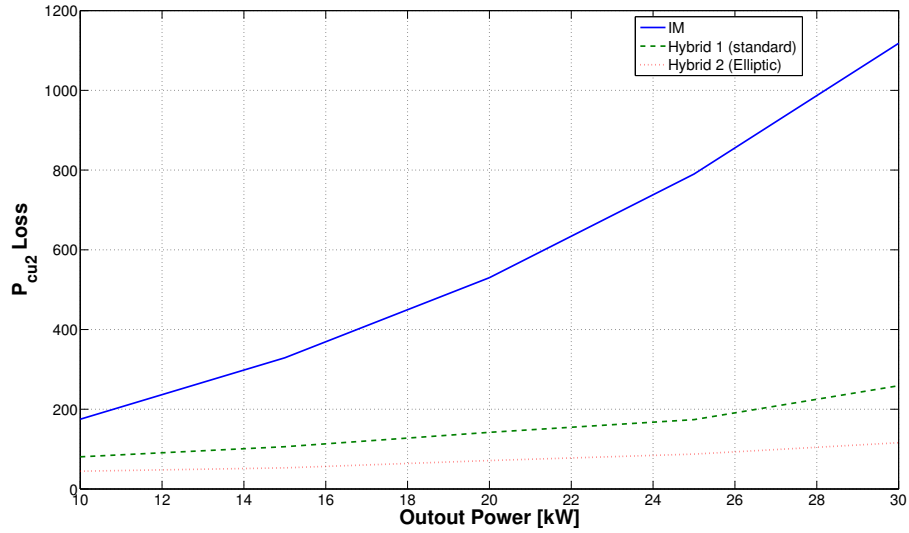


Figure 5.28: P_{cu2} loss comparison at different power levels.

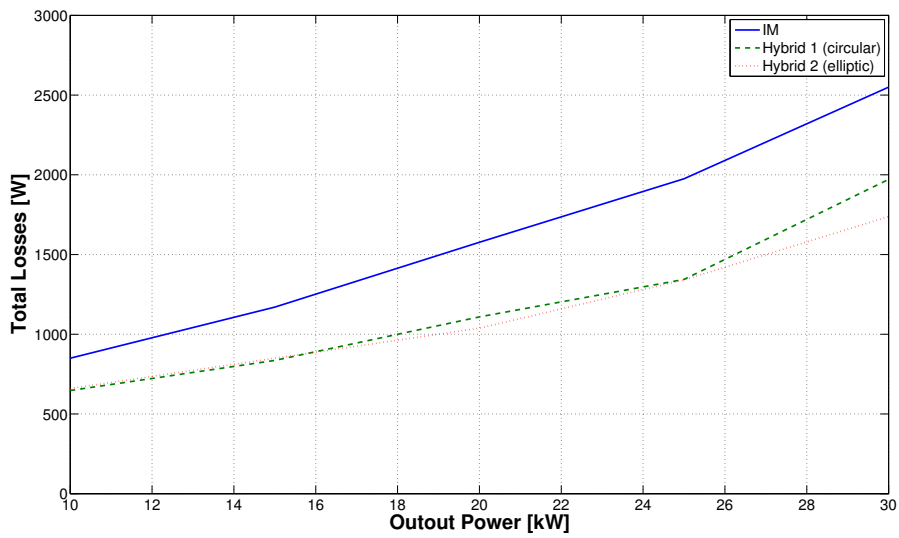


Figure 5.29: Total losses comparison at different power levels.

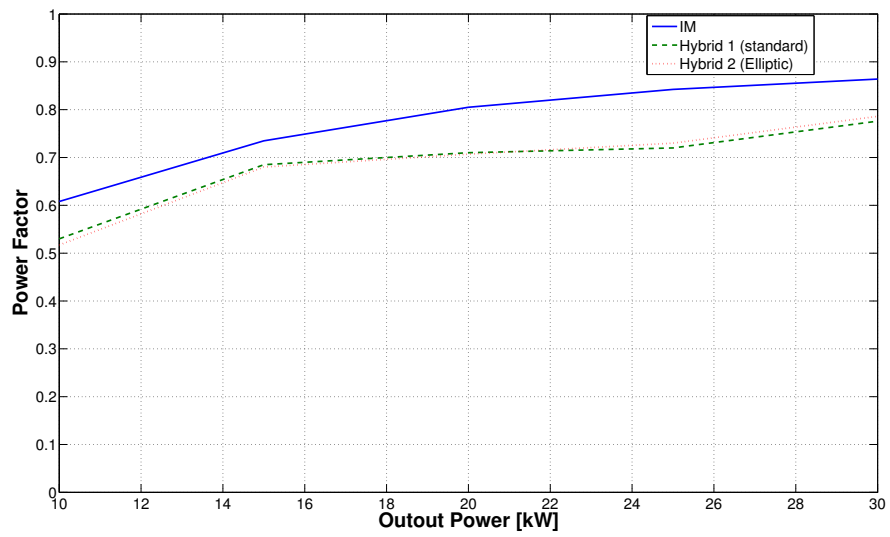


Figure 5.30: PF comparison at different power levels.

5.4 Performance summary

In order to compare the different designs of the hybrid concept with the IM, all important results are summarized in Table 5.4

Table 5.4: Performance comparison

Motor type	IM	SynRM	Hybrid 1, (standard)	Hybrid 2
Frequency [Hz]	50	50	50	50
Speed [rpm]	1466	1500	1500	1500
Slip [%]	2.24	0	0	0
Starting time [ms]	51.1	N/A	67.5	74.8
V_{rms} [V]	400	400	400	400
I_{rms} [A]	39.9	40.2	41.7	40.7
Stator Cu Losses [W]	694	682	721	688
Stator iron Losses [W]	196	186	174	183
Rotor Cu Losses [W]	530	0	142	71
Rotor iron Losses [W]	52	76	72	75
Mechanical Losses [W]	100	100	100	100
Total Losses [W]	1578	1044	1209	1117
Torque [Nm]	130	127	127	127
Torque ripple* [%]	35	19.7	17.5	16.6
P_{in} [kW]	21503	20848	21226	20858
P_{out} [kW]	19925	19804	20017	19741
PF	0.736	0.707	0.710	0.707
Efficiency [%]	92.66	95.00	94.30	94.64
Efficiency · PF	0.68	0.67	0.67	0.67

*No skew

6

Conclusion

The hybrid motor is able to synchronize and keep the combined good properties from both the IM and SynRM.

If the hybrid arrangement is not able to synchronize the speed and moving torque will start oscillating which will lead to great losses and vibrations in the setup.

It also seems like the starting position of the rotor does not impact whether or not the motor will synchronize.

The amount of aluminium does not have a significant influence on the starting performance.

The placement has a big impact on both the starting and losses. If the cage bars are placed close to the rotor periphery the starting torque is increased but steady state efficiency is reduced.

The investigation of number of barriers followed what other reports suggested i.e. four barriers with a non cut-off rotor structure. A conclusion about the number of barriers is vague but it seems to be possible with 3-6 number of barriers.

Another influence investigated was the open end barrier. This indicated that more current was induced in the rotor cage when the barriers did not have any bridges. It gives rise to torque oscillation and additional losses in steady state.

The efficiency class is increased from IE3 to IE4 by the solid loss decrement in the rotor cage. The losses in the rotor is reduced to 70 W from over 500 W with the hybrid

arrangement compared to the IM.

6.1 Discussion

This project has aimed to verify the LS-SynRM concept rather than to optimize the design. Since the focus has been on finding an efficient line start design of the hybrid motor the design of the induction motor is not as good as it could be. The results still indicate that there is great potential in this kind of arrangement. The stator structure has not been optimized at all and could probably be improved to increase the performance in all designs. The thesis also focus on how certain parameters affects the performance. Parametric sweeps outside the range investigated in this report may show better results than presented here.

The purpose to achieve direct line-start capability is to make the motor independent of peripheral devices, however there is a need for some kind of safety device in case the motor does not synchronize. The oscillations in case of synchronizing failure would most likely damage the motor severely. Furthermore, there is a need for future evaluation in both the SynRM rotor design and the rotor cage to find an efficient LS-SynRM.

6.2 Future Work

In order for the hybrid arrangement to be competitive in industrial applications there is a necessity to improve especially the power factor but also and consequently the efficiency. Another competitor is the Permanent Magnet Synchronous Machine, PM-assisted LS-SynRM, which can successfully be combined with both the SynRM and Hybrid motor. The immediate gain is higher power factor and higher efficiency but other possibilities are better torque density and lower torque ripple. However, by introducing permanent magnets, the motor will be more expensive and complicated. An alternative in design flexibility is by mounting PMs into the empty space inside the barriers depending on what performance that is demanded by the application. Other areas that needs to be evaluated which this thesis did not include is the mechanical and thermal properties of the motor. A study of this should show the need for reinforcing bridges over the barriers, how they should be placed and how the aluminum and steel expands during operation.

A

Induction Machine data for analytical solution

GENERAL DATA

Given Output Power (kW):	20
Rated Voltage (V):	400
Winding Connection:	Wye
Number of Poles:	4
Given Speed (rpm):	1470
Frequency (Hz):	50
Stray Loss (W):	200
Frictional Loss (W):	50
Windage Loss (W):	50
Operation Mode:	Motor
Type of Load:	Fan Load
Operating Temperature (°C):	75

APPENDIX A. INDUCTION MACHINE DATA FOR ANALYTICAL SOLUTION

STATOR DATA

Number of Stator Slots:	36
Outer Diameter of Stator (mm):	254
Inner Diameter of Stator (mm):	165
Type of Stator Slot:	4
Stator Slot	
<hr/>	
hs0 (mm):	0.7
hs1 (mm):	0.8
hs2 (mm):	19.9254
bs0 (mm):	3.9
bs1 (mm):	7.16595
bs2 (mm):	10.6524
rs (mm):	0.2
Top Tooth Width (mm):	7.49946
Bottom Tooth Width (mm):	7.49946
Length of Stator Core (mm):	205
Stacking Factor of Stator Core:	0.96
Type of Steel:	M19_24G
Number of lamination sectors	0
Press board thickness (mm):	0
Magnetic press board	No
Number of Parallel Branches:	1
Type of Coils:	21
Coil Pitch:	8
Number of Conductors per Slot:	12
Number of Wires per Conductor:	1
Wire Diameter (mm):	3.264
Wire Wrap Thickness (mm):	0

APPENDIX A. INDUCTION MACHINE DATA FOR ANALYTICAL SOLUTION

Wedge Thickness (mm):	0
Slot Liner Thickness (mm):	0.1
Layer Insulation (mm):	0.1
Slot Area (mm ²):	187.821
Net Slot Area (mm ²):	173.211
Slot Fill Factor (%):	73.8085
Limited Slot Fill Factor (%):	85
Wire Resistivity (ohm.mm ² /m):	0.0217
Conductor Length Adjustment (mm):	0
End Length Correction Factor	1
End Leakage Reactance Correction Factor	1

APPENDIX A. INDUCTION MACHINE DATA FOR ANALYTICAL SOLUTION

ROTOR DATA

Number of Rotor Slots:	28
Air Gap (mm):	0.55
Inner Diameter of Rotor (mm):	45
Type of Rotor Slot:	1
Rotor Slot	
<hr/>	
hs0 (mm):	0.35
hs01 (mm):	0.35
hs2 (mm):	0
bs0 (mm):	0
bs1 (mm):	7.5
bs2 (mm):	7.5
Type of Rotor Bottom Slot:	4
Rotor Bottom Slot	
<hr/>	
hs0 (mm):	1.5
hs1 (mm):	1
hs2 (mm):	18
bs0 (mm):	2
bs1 (mm):	6.7
bs2 (mm):	2
rs (mm):	1
Cast Rotor:	No
Half Slot:	No

APPENDIX A. INDUCTION MACHINE DATA FOR ANALYTICAL SOLUTION

Length of Rotor (mm):	205
Stacking Factor of Rotor Core:	0.92
Type of Steel:	M19_24G
Skew Width:	0
End Length of Bar (mm):	0
Height of End Ring (mm):	50
Width of End Ring (mm):	15
Resistivity of Rotor Bar at 75 Centigrade (ohm.mm ² /m):	0.0434783
Resistivity of Rotor Ring at 75 Centigrade (ohm.mm ² /m):	0.0434783
Magnetic Shaft:	Yes

Bibliography

- [1] ABB, IE4 synchronous reluctance motor and drive package Optimized cost of ownership for pump and fan applications (2012).
- [2] J. Minx, K. Scott, et. al, An analysis of Sweden's carbon footprint, Tech. rep., WWF Sweden (2008).
- [3] The Commission of the European Communities, Commission regulation (EC) No 640/2009 (July 2009).
- [4] H. Nam, S. B. Park, G. H. Kang, J. Hong, J. B. Eom, T. Jung, Design to improve starting performance of line-start synchronous reluctance motor for household appliances, Industry Applications Conference, 2004. 39th IAS Annual Meeting. Conference Record of the 2004 IEEE Vol. 1 (2004) 79–85.
- [5] M. Gamba, G. Pellegrino, A. Vagati, F. Villata, Design of a line-start synchronous reluctance motor, Electric Machines Drives Conference (IEMDC), 2013 IEEE International (2013) 648–655.
- [6] D. Miljavec, M. Zagirnyak, B. Zidaric, Rotor-design and on-line starting-performance analysis of a synchronous-reluctance motor, The international journal for computation and mathematics in electrical and electronic engineering Vol. 28 (No. 3) (2009) 570–582.
- [7] I. Boldea, S. A. Nasar, The Induction Machines Design Handbook, Second Edition, CRC Press, 2009.
- [8] A. R. Gallego, Design and optimization of an IE4 4-pole 7.5 kW induction motor, Degree project, The Royal Institute of Technology, KTH, Stockholm, Sweden (2014).
- [9] J. K. Kostko, Polyphase Reaction Synchronous Motors, Journal of the American Institute of Electrical Engineers Vol. 42 (No. 11) (1923) 1162–1168.
- [10] R. R. Moghaddam, Synchronous reluctance machine in variable speed drives applications, PhD thesis, The Royal Institute of Technology, KTH (May 2011).

- [11] H. Lendenmann, R. R. Moghaddam, A. Tammi, L. E. Thand, Motoring Ahead, Review 1, ABB (April 2011).
- [12] R. R. Moghaddam, Synchronous reluctance machine (SynRM) design, Master thesis, The Royal Institute of Technology, KTH (2007).